MDPI

Review

Recent Advances in Photocatalytic Degradation of Tetracycline Antibiotics

Jiale Ma [1], Yang Chen [1], Gang Zhou [2], Haiyu Ge [3] and Hongbo Liu [1,*]

[1] School of Environment and Architecture, University of Shanghai for Science and Technology, 516 Jungong Road, Shanghai 200093, China; mjl_ssll@163.com (J.M.); cy1096325538@163.com (Y.C.)
[2] Zhejiang Province Environmental Engineering Co., Ltd., 9 Huanggushan Road, Hangzhou 310012, China; 13588134056@126.com
[3] School of Architecture and Civil Engineering, West Anhui University, Lu'an 237012, China; gehy@wxc.edu.cn
[*] Correspondence: liuhb@usst.edu.cn

Abstract: China is a significant global producer and consumer of pesticides and antibiotics, with their excessive use leading to substantial water pollution that poses challenges for subsequent treatment. Photocatalytic degradation, leveraging renewable solar energy, presents an effective approach for decomposing organic pollutants and reducing residual contaminant levels in water bodies. This approach represents one effective way for addressing environmental challenges. This paper classifies representative photocatalytic materials by structural design and degradation principles including MOFs (Metal–Organic Frameworks), metal- and nonmetal-doped, mesoporous material-loaded, carbon quantum dot-modified, floatation-based, and heterojunction photocatalysts. We also discuss research on degradation pathways and reaction mechanisms for antibiotics. Of particular importance are several key factors influencing degradation efficiency, which are summarized within this work. These include the separation and charge transfer rate of catalyst surface carriers, and the wide-spectrum response capabilities of photocatalysts, as well as persulfate activation efficiency. Furthermore, emphasis is placed on the significant role played by intrinsic driving forces such as built-in electric fields within catalytic systems. Moreover, this paper introduces several promising composite-structure photocatalytic technologies from both composite-structure perspectives (e.g., Aerogel-based composites) and composite-method perspectives (e.g., the molecularly imprinted synthesis method). We also discuss their latest development status, along with future prospects, presenting valuable insights for pollutant degradation targets. This work aims to facilitate the design of efficient photocatalytic materials, while providing valuable theoretical references for environmental governance technologies.

Keywords: tetracycline antibiotics; photocatalysis; novel composite photocatalyst; degradation mechanism

1. Introduction

Over the past few decades, rapid industrial activities have raised significant concerns regarding environmental pollution, water scarcity, and climate change. Emerging pollutants in water resources exhibit varying degrees of toxic effects on human, animal, and plant life. A substantial portion of industrial wastewater is discharged into the environment without adequate treatment. This untreated wastewater often contains pollutants such as pharmaceuticals, dyes, personal care products, and pesticides. These contaminants pose serious direct or indirect risks to both human health and the environment [1].

Recent years have seen antibiotics emerge as a new category of organic pollutants in natural water environments. This issue has gained significant interest [2]. As drugs for the treatment of infectious diseases, they are widely used in large quantities and have an important place in medicine. However, due to the limited absorption capacity of antibiotics in the animal intestine, most antibiotics applied to animals (about 30–90 percent) are

excreted into the environment in the form of parent structures or metabolites through urine or feces [3]. At the same time as drugs that inhibit the growth of microorganisms, antibiotics in the natural aquatic environment have toxic effects on certain organisms, thus affecting their normal growth or reproduction [4]. The widespread use of antibiotics has led to the accumulation of antibiotic-resistant bacteria (ARB) and antibiotic-resistant genes (ARGs) in the environment, posing a potential threat to ecosystems and human health [5]. Consequently, the extensive use of antibiotics can facilitate their entry into the environment through direct or indirect pathways, resulting in environmental pollution and posing risks to the health of biological organisms.

Tetracyclines (TCs) are a class of broad-spectrum antibiotics produced by actinomycetes, which are inexpensive and are currently one of the most widely used and densely used types of antibiotics in the world. Studies have shown that TCs can enter the environment through a variety of pathways, including medical care, aquaculture, and animal husbandry, inducing the production and spread of TC-resistant genes [6]. At the same time, data show that TCs can produce toxic effects on non-target organisms, pose potential hazards to aquatic organisms in the environment, and can even enter the food chain through the enrichment of aquatic animals, which in turn affects human health [7]. Currently, antibiotic resistance has been classified as a global threat to human health by the WHO [8]. Therefore, it is necessary to develop advanced sustainable technologies to purify antibiotics in water resources [9]. Over the past decades, a number of approaches have been used to address the problem of antibiotic residues in wastewater [10,11]. In recent years, tetracycline antibiotics have been frequently detected in water bodies. In particular, oxytetracycline (OTC) and chlortetracycline (CTC), are commonly found in aquatic environments. Their presence in wastewater treatment plants is influenced by local climate, population density, wastewater volume, and antibiotic usage. Conventional treatment methods remove only 36–79% of TCs [12], leaving residues that inhibit aquatic organism growth and may accumulate in the food chain, posing health risks such as joint disease, kidney problems, endocrine disruption, and mutagenicity [13]. In soils and sediments, TCs, primarily OTC, are present in concentrations ranging from ng/kg to mg/kg [14]. Tetracycline contamination from manure and fertilizers releases antibiotics into soil, along with transformation products (TPs) like 4-epi-tetracycline and dehydrotetracycline [15]. Exceeding a threshold of 100 μg·kg-1, as recommended by the Veterinary International Conference on Harmonization (VICH), can cause irreversible ecological harm, impacting the growth, reproduction, and survival of aquatic species, especially fish, crustaceans, and plankton. This can lead to reproductive suppression, altered behaviors, and reduced population sustainability, while fostering antibiotic-resistant bacteria, further disturbing microbial ecosystems and exacerbating resistance issues.

Major removal methods for tetracycline-contaminated wastewater include physicochemical and biological processes. Physicochemical techniques, such as coagulation-sedimentation, membrane separation, and adsorption, achieve only 50% to 60% removal efficiency without altering the chemical structure of TCs [16]. Membrane technologies, particularly nanofiltration and reverse osmosis are promising [17]. Ozone can oxidize tetracycline, with higher efficiency under acidic conditions, but still faces challenges in degradation efficiency and mineralization rates. Electrochemical oxidation generates hydroxyl radicals (·OH) for degradation, but is limited by high energy consumption and toxic intermediates [18]. Photo-Fenton combines photolysis and the Fenton reaction to produce reactive hydroxyl radicals, effectively degrading TCs into smaller molecules or mineralizing it into CO_2 and water. This method is environmentally friendly and cost-effective, but its success relies on the efficiency of photocatalysts, highlighting the need for improved catalytic materials.

Photocatalytic degradation technology is an efficient, environmentally friendly, and cost-effective degradation method. It uses solar irradiation as energy and employs the strong redox properties of electron-hole pairs in photocatalysts for degradation. This process can degrade typical antibiotics, such as tetracycline, into carbon dioxide and water,

without the need for additional oxidants or reductants, effectively addressing the spread of antibiotic resistance [19]. However, traditional photocatalytic systems greatly depend on the band structure and surface structure of the catalyst. Issues such as slow separation of electron-hole pairs and limited active surface sites lead to subpar performance [20]. Despite significant efforts, most research remains confined to conventional single-component photocatalysts and composite photocatalysts. The fast photogenerated carrier-complexation rate, limited light-trapping range, low charge-transfer efficiency and low radical-generation efficiency of single-component photocatalysts have severely limited their application in water treatment [21,22].

However, current research primarily focuses on specific types of photocatalysts for the degradation of particular pollutants. There remains a lack of comprehensive summaries regarding the variety of novel photocatalysts and their mechanisms for degrading tetracycline. Only a few studies thoroughly cover emerging photocatalytic materials and their applications in some typical antibiotics. However, this information is crucial to affirm their practical superiority and effectiveness as photocatalysts for photodegradation. Therefore, reviewing the latest advancements and mechanisms of novel photocatalysts in the catalytic oxidation process of tetracycline, a typical antibiotic pollutant, becomes particularly significant.

This review offers a thorough analysis of recent progress in the photocatalytic degradation of TCs. Initially, it categorizes photocatalysts based on type, element composition, and structure, clarifying their relationship with performance. It provides a concise overview of various photocatalytic principles and their fundamental applications in tetracycline antibiotic degradation. Subsequently, it delves into six distinct types of photocatalytic materials that can be seen in Figure 1 below, assessing their effectiveness against these antibiotics. The review also summarizes the degradation pathways and mechanisms involved, while highlighting critical factors that influence degradation efficiency. Finally, it explores the future potentials of photocatalytic technology, considering the current research landscape and application trends of emerging materials. The review on the photocatalytic degradation of tetracycline antibiotics aims to offer theoretical insights and practical direction to advance environmental treatment technologies, addressing the growing challenges of environmental pollution.
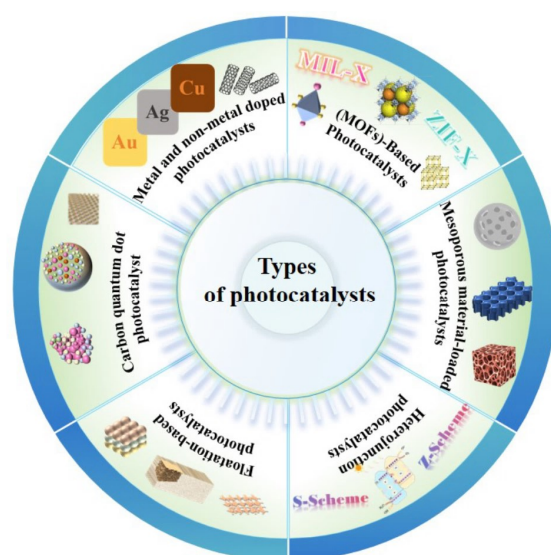

Figure 1. Different types of photocatalytic materials for tetracycline antibiotic degradation in this review.

2. Photocatalytic Materials for Tetracycline Antibiotic Degradation

In order to improve the photocatalytic efficiency, researchers have recently focused on the composite modification of single-component photocatalysts to enhance their catalytic

performance by expanding the light absorption range, improving the photogenerated carrier-separation efficiency, and increasing the number of active sites, as well as enhancing the redox ability [23]. Liu et al. synthesized MOF-BiOCl S-type heterojunction composites in situ by the halogenation technique [24]. Li et al. synthesized Sulfur-doped algal graphite carbon nitride photocatalysts by microwave [25]. Zhang et al. successfully prepared ultrathin nanosheet photocatalysts (FCNN-X) with enhanced multi-electron transfer and molecular oxygen activation by interspersing FeOOH QDs and CQDs in g-C_3N_4 based on the principle of dual-quantum-dot co-photocatalysts to promote photocatalysis in 0D/2D heterojunction photocatalysts [26]. To enhance the efficiency of photocatalytic degradation of tetracycline, single-component photocatalytic materials can be modified through methods such as elemental doping, morphological optimization, and in situ growth, etc. Furthermore, improving photoelectron transfer, enhancing visible light absorption, and increasing specific surface area can elevate the availability of active reaction sites, thereby promoting overall photocatalytic performance. The photocatalysts are categorized in detail, as follows.

2.1. Metal-Organic Framework (MOF)-Based Photocatalysts

MOFs are a class of novel materials characterized by a porous network structure, formed by metal ions acting as nodes and organic ligands serving as linkers [27]. In general, photocatalytic reactions involve the excitation of a photocatalyst by light, resulting in the generation of photoinduced charge carriers that subsequently participate in redox reactions [28]. Currently, there are generally two theories to explain the mechanism of MOF photocatalysis [29]. (1) Photo-induced charge separation occurs when metal clusters and photoactive ligands absorb incident light. This absorption excites electrons from the valence band (VB) to the conduction band (CB), generating free electrons in the CB. Simultaneously, free holes are created in the VB. These photo-generated electron holes migrate to the surface of the photocatalyst, where they actively participate in redox reactions. (2) The highest occupied molecular orbital–the lowest unoccupied molecular orbital (HOMO-LUMO) theory and ligand charge-transfer mechanisms in MOF-based photocatalysts reveal that the metal clusters in MOFs, similar to isolated semiconductor quantum dots, can accept electrons from organic ligands, which serve as connectors. Due to the presence of multiple catalytic sites, traditional semiconductor theories alone cannot fully explain MOF photocatalysis. Various charge transfer pathways, such as ligand-to-ligand charge transfer (LLCT), ligand-to-metal charge transfer (LMCT), metal-to-metal-to-ligand charge transfer (MMLCT), and metal-to-ligand charge transfer (MLCT) and facilitate photoexcitation. In LMCT, electrons transfer from the ligand's HOMO to the metal's LUMO, enhancing charge separation and photocurrent density, ultimately improving the catalytic efficiency of MOFs [30]. In recent years, Metal–Organic Frameworks (MOFs) have raised significant interest from researchers in the field of photocatalysis, due to their high specific surface area, tunable porosity, and unsaturated active sites [31,32]. Wang et al. synthesized a $Bi_{12}O_{17}Cl_2$ photocatalyst through the hydrolysis of bismuth-based metal organic framework (Bi-BTC) precursors under visible light, resulting in nanosheets with superior photocatalytic activity for tetracycline hydrochloride degradation compared to conventional materials [33]. A controlled self-assembly hydrothermal method effectively coupled crystalline Fe/Mn-MOF with CdS particles, enhancing the distribution of CdS on the MOF surface [34]. This integration not only increased the number of active sites, but also improved the migration efficiency of photogenerated carriers, thereby enhancing photocatalytic performance. Additionally, Xu et al. developed BiOCl-based photocatalysts with a double Z-scheme heterojunction structure, utilizing Bi-MOF as a template, which showed remarkable degradation efficiency for tetracycline under simulated sunlight [35]. MOFs also emerge as promising hosts. They enable the design and synthesis of efficient photocatalysts featuring heteroatomic metal nodes, through the incorporation of iron components [36]. Fe-MOFs are considered as highly promising photo-Fenton photocatalysts, due to their excellent visible-light trapping ability and highly dispersed iron active sites. Chen et al. proposed that three iron-based

MOFs (MIL-53, MIL-88B, and MIL-101) and their annealed derivatives (collectively referred to as Fe-MIL) with the same composition possessed the ability to thermally catalyze the TC degradation, with the best sample showing a degradation efficiency of 94.22% of TCs within 60 min at 70 °C [37].

At the same time, the flexibility of MOFs in structure and chemical properties facilitates their modification [38]. They can be synthesized under controlled conditions, exhibiting good specificity and selectivity. In recent years, novel S-type heterojunction structures have significantly mitigated the issue of carrier recombination, while maintaining a high oxidation–reduction potential, thereby enhancing the performance of photocatalysts. An S-type heterojunction typically consists of an oxidation photocatalyst (OP) characterized by a higher valence band (VB) energy and a lower Fermi level (E_f), combined with a reduction photocatalyst (RP) that possesses a lower conduction band (CB) energy and a higher Fermi level (E_f). There is an "S"-shaped charge carrier transfer path with photo-generated carriers at the interface, and it has a high oxidation–reduction capacity. By combining these two features to construct MOF-based S-type heterojunction photocatalysts, not only can the excellent properties of MOFs be maintained, but the S-type charge transfer path can also be realized [39,40]. Luo et al. synthesized the MOF-545/Ag_3PO_4 photocatalyst by the solvothermal method, which has stronger light response and charge separation ability than the single Ag_3PO_4 catalyst [41]. Table 1 provides a summary of recent studies conducted over the past two years on the degradation of TCs and TCH in aquatic environments using (MOF)-based photocatalysts.

Table 1. Degradation of TCs and TCH by Metal–Organic Framework (MOF)-based photocatalysts.

Pollutants	Materials	Band-Gap Energy (eV)	Degradation Condition			Degradation Efficiency	Ref.
			Time/min	Catalyst Dosage	Concentration of Pollutants (mg/L)		
TCs	$Bi_{12}O_{17}Cl_2$	2.20	60	20 mg	20	92.2%	[36]
TCH	Bi/CeO_2 (BC-1000)	2.99	90	15 mg	10	91.89%	[42]
TCs	$BaTi_{0.85}Zr_{0.15}O_3$/MOF-5	2.86	150	200 mg/L	10	95%	[43]
TCs	ZIF-67embedded Bentonite/alginate beads (ZIF-AB 2.5)	-	60	500 mg/L	25	99.8%	[44]
TCs	Al-MOF/MoS_2/WS_2 (AlMWS)	3.26	75	300 mg/L	30	97.93%	[45]
TCs	CQD@UiO-66-NH_2/PSF	-	-	500 mg/L	20	100%	[46]
TCs	Cu@UIO-66-NH_2/$ZnIn_2S_4$	-	120	20 mg	20/40	92.6%	[47]
TCs	Ni/Mn-MOF-74/CdS@Co_3O_4 (4:4) (MCC-4)	-	70	50 mg	40	99.2%	[48]
TCs	NH_2-ML-101 (Fe^{2+}/Fe^{3+})-0.2	2.27	90	25 mg	20	94%	[49]
TCH	FeMn-PBA@MXene-0.30	3.36	120	200 mg	30	93.41%	[50]

2.2. Element-Doped Photocatalysts

Element doping can modulate the optical and electrical properties of semiconductors as well as their band structure, and is regarded as an effective strategy for enhancing the light absorption and charge carrier transport capabilities of photocatalysts [51]. Dopants can reduce the bandgap energy of titanium dioxide by introducing additional states within the bandgap, enhancing visible light absorption. Various dopants (metals, non-metals, and their combinations) can alter the morphology and optical/electrical properties of semiconductor particles, thereby improving their photocatalytic activity under visible light [47]. Commonly used dopants in photocatalysis include Al [52], Fe [53], Mn [54], Mo [55] and Ce [56], or doping semiconductors (e.g., TiO_2 [52], CeO_2 [56] and g-C_3N_4 [55]). An Al-doped TiO_2 photocatalyst was synthesized via an evaporation-induced process, resulting in a black TiO_2 that exhibited extended light absorption and abundant oxygen vacancies after reduction. This photocatalyst demonstrated notable degradation of tetracycline hydrochloride [52]. Similarly, a hollow microsphere structure of Fe-doped TiO_2 was developed for efficient photocatalytic-Fenton degradation under visible light, enhancing light absorption and reducing electron–hole recombination [53].

Additionally, manganese zinc ferrite photocatalysts with spin polarization effects showed improved TC removal when subjected to an external magnetic field [54]. A mechanical activation treatment followed by calcination was used to create a MoO_2/Mo-doped g-C_3N_4 Schottky heterojunction composite, which exhibited exceptional photocatalytic efficiency and structural stability for tetracycline degradation [55]. A Ce-doped $CdIn_2S_4$ photocatalyst was synthesized using a modified co-precipitation method. The decomposition products of CeO_2 are present in the supernatant as Ce(III) ions, significantly enhancing the specific surface area of the photocatalyst and increasing the availability of active sites for reactant interaction [56]. Table 2 provides a summary of recent studies conducted over the past two years on the degradation of antibiotic pollutants in aquatic environments using element-doped composite photocatalysts.

Table 2. Degradation of TCs and TCH by element-doped composite photocatalysts.

Pollutants	Materials	Band-Gap Energy (eV)	Degradation Condition			Degradation Efficiency	Ref.
			Time/min	Catalyst Dosage	Concentration of Pollutants (mg/L)		
TCH	Ce/Bi_2WO_6	1.61	40	600 mg/L	35	90.40%	[57]
TCs	$Ce-Fe/CaWO_4$	2.10	120	500 mg/L	10	98.4%	[58]
TCs	Mn-Fe/CN-50	1.80	50	400 mg/L	20	99%	[59]
TCH	Ce5-CdS/N-rGO20	-	90	500 mg/L	20	94.5%	[60]
TCs	Mn-FeOOH/CNNS	-	50	300 mg/L	20	99.7%	[61]
TCs	Cu/Bi_2O_2S	-	30	30 mg	30	90.4%	[62]
TCs	$Co/BiVO_4$-Vo	2.28	10	200 mg/L	20	92.3%	[63]
TCH	$Yb_{0.4}/BiOBr$	2.95	100	200 mg/L	20	89.38%	[64]
TCH	$La/FeTiO_3$	2.47	120	-	20	91.38%	[65]
TCs	$Bi_{0.05}La_{0.95}Cu_{0.1}Fe_{0.9}O_3$	2.39	60	100 mg	40	94.6%	[66]

Doping photocatalysts with metal ions can introduce intermediate energy levels within the material, resulting in a narrower bandgap and an expanded range of light absorption. Furthermore, the strong electron-capturing capability of metal ions facilitates the accumulation of photo-generated electrons in their vicinity, thereby enhancing the separation efficiency of electron–hole pairs and significantly improving photocatalytic activity [67]. Qu et al. synthesized a visible-light-responsive composite photocatalyst, the K-doped g-C_3N_4/BiOBr [68]. Photocurrent and electrochemical experimental results demonstrate that the incorporation of K effectively reduces the bandgap of the g-C_3N_4/BiOBr composite material and enhances the separation efficiency of photogenerated charge carriers, leading to efficient degradation of tetracycline hydrochloride (TCH).

In comparison to metal ions, non-metal ions are less prone to forming complex centers and do not deplete light-induced charges, thereby enhancing photocatalytic activity more effectively [69]. To enhance absorption in the visible region, a viable approach is to moderately narrow the bandgap by introducing localized electronic energy levels within the forbidden band. Common methods include lattice gap doping and substitutional doping of oxygen atoms with non-metallic elements. Frequently used dopants include N, S, C, B, P and F. Nitrogen doping is particularly prevalent, due to its diverse sources and effective bandgap optimization [70]. Tao et al. developed a nitrogen-doped reduced TiO_2 porous photocatalyst using atmospheric plasma spraying (APS) technology combined with geometric concepts, achieving synthesis in just 15 min. The narrower band-gap values enable more effective utilization of visible and near-infrared light, decreasing the recombination rate of photogenerated electrons and holes, and facilitating the photocatalytic reaction [71].

2.3. Mesoporous Material-Loaded Photocatalysts

Mesoporous materials (with pore sizes ranging from 2 to 50 nm) are increasingly recognized as highly promising carriers for the immobilization of photocatalysts, owing to their distinctive porous architecture. This structure confers several advantages over non-porous supports, including the mitigation of catalyst agglomeration and an enhancement in charge transfer rates, both of which significantly improve catalytic efficiency. Furthermore, the

mesoporous framework and interconnected pore channels facilitate the uniform dispersion of granular photocatalysts across their surfaces or within their pores. This effectively addresses the challenge posed by agglomeration in single-component photocatalysts that hinders light absorption at active sites. Consequently, this configuration allows for optimal interaction between the catalyst and substrate, thereby enhancing mass-transfer and diffusion processes critical for efficient photocatalytic activity [72].

Currently, commonly used mesoporous materials include mesoporous carbon-based materials, metal oxides, and MOFs [73–75]. Maliheh et al. employed SiO_2 clusters as templates to synthesize mesoporous graphitic carbon nitride nanoclusters (NCMCN), which exhibited exceptional photocatalytic performance, achieving complete degradation of TC solution within 30 min [76]. Tang et al. constructed a 2D/2D CeO/BiOCl S-type photocatalyst consisting of mesoporous CeO and BiOCl nanosheets (NSs) [77], which exhibited excellent photocatalytic activity for four antibiotics, TCs, chlortetracycline (CTC), doxycycline (DOC), and oxytetracycline (OTC). A simple method for synthesizing a ternary nanocomposite comprising strontium oxide-modified mesoporous graphitic carbon nitride supported on titanium dioxide (SrO-mpg-CN/TiO_2) has been developed. This nanocomposite demonstrates significant efficiency as a heterojunction photocatalyst for the degradation of tetracycline antibiotics [78]. The doping of rare-earth elements is capable of modifying the crystal lattice structure, generating defects, facilitating the in situ creation of oxygen holes within the crystal, augmenting the bandgap, and expanding the light absorption range from localized areas to the entire spectrum. Additionally, among various functional energy materials, mesoporous crystalline framework materials (MCFs) with pore diameters of 2 to 50 nm and crystallized pore walls are recognized for their significant potential in energy applications, due to their exceptional physical properties. MCFs typically feature a high surface area and accessible mesoporosity for reactants, as well as semiconductor walls that enable photoelectric conversion. By fine-tuning the pore structure or other intrinsic characteristics, photocatalytic performance can be notably enhanced [79]. In recent decades, the importance of nanostructures in developing novel high-performance mesoporous materials has become increasingly evident. Several synthetic methods have been developed to control the size and morphology of MCFs, including zero-dimensional particles, one-dimensional nanorods, two-dimensional nanosheets, and three-dimensional nanospheres. Table 3 provides a summary of recent studies conducted over the past two years on the degradation of TCs and TCH in aquatic environments using mesoporous material-loaded photocatalysts.

Table 3. Degradation of TCs and TCH by mesoporous material-loaded photocatalysts.

Pollutants	Materials	Band-Gap Energy (eV)	Degradation Condition			Degradation Efficiency	Ref.
			Time/min	Catalyst Dosage	Concentration of Pollutants (mg/L)		
TCs	Mesoporous I-doped g-C_3N_4 with 0.50 g of I dopant (GCN-I0.50)	2.45	150	600 mg/L	10	99.8%	[80]
TCs	nanoporous-TiO_2-encapsulating macroporous-double-gyroid-structure photocatalyst (TiO_2@DGS)	2.82	60	-	10	93.6%	[81]
TCs	$Ti_{0.95}Ru_{0.05}O_{2-y}$	-	50	20 mg	10	98.7%	[82]
TCs	B-g-C_3N_4/SBA-15 [a]	2.19	120	10 mg	20	93.74%	[83]
TCs	$MnCo_2O_4$/TiO_2	2.13	60	160 mg/L	20	100%	[84]
TCs	HCOF-Ph@g-C_3N_4 (HCg-30% [b])	-	14	30 mg	30	100%	[85]
TCs	porous molybdenum graphene aerogel (pMGA)	-	120	500 mg/L	5	97%	[86]
TCH	CsPbBr$_3$@HZIF-8 (the hierarchically porous ZIF-8)	-	40	15 mg	10	94%	[87]

Table 3. *Cont.*

Pollutants	Materials	Band-Gap Energy (eV)	Degradation Condition			Degradation Efficiency	Ref.
			Time/min	Catalyst Dosage	Concentration of Pollutants (mg/L)		
TCs	1-CN@BCO (CN:BO/BCO=1:1)	2.56	40	200 mg/L	20	98.1%	[88]
TCs	LDH-SnO$_2$-WO$_3$ (LDH, Layered double hydroxides)	3.69	120	-	20	95.5%	[89]

[a] SBA-15 is a kind of mesoporous molecular sieve. [b] 30% is the mass fraction of g-C$_3$N$_4$.

However, several elements remain unaddressed. Key drawbacks include low thermal stability, leading to unexpected collapse at high temperatures, and a fragile framework that cannot withstand significant strains. Fewer than 30 metal elements can form mesoporous crystalline frameworks (MCFs), most relying on aggregation mechanisms for structure formation. Only a small fraction of these can effectively assemble with templates to produce well-defined MCFs.

2.4. Carbon Quantum Dot Photocatalyst

In recent decades, fluorescent quantum dots have gained significant attention for their tunable optoelectronic properties [90]. They can be categorized into polymer dots (PDs), graphene quantum dots (GQDs), and carbon quantum dots (CQDs). Among these, CQDs are ideal alternatives to traditional quantum dots, due to their non-toxic carbon sources and simple synthesis methods, addressing environmental concerns. CQDs inherit the superior upconversion photoluminescence and stability of conventional quantum dots, while offering excellent chemical stability and water solubility. Their outstanding electronic properties and biocompatibility enable applications in biological imaging, chemical sensing, optoelectronics, and photocatalysis.

Zhang et al. developed a nitrogen-doped carbon quantum dot (N-CQD)-modified oxygen vacancy CuFe$_2$O$_4$/nitrogen vacancy g-C$_3$N$_4$ (CFOv/NvCN) composite material [91]. Carbon quantum dots efficiently connect two semiconductors, enabling swift transport of electron–hole pairs. This promotes rapid movement of photogenerated carriers and facilitates efficient degradation of TCs in a short time-frame. Gandharve Kumar et al. presented a highly efficient approach for the photocatalytic degradation of tetracycline and ciprofloxacin in aqueous media, utilizing an optimized nanocomposite of silicon-doped carbon quantum dots (1.0SiCQDs) decorated on bismuth molybdate (Bi$_2$MoO$_6$) as a solar photocatalyst. This photocatalyst is synthesized through a hydrothermal method [92]. In addition, novel composite photocatalysts modified with carbon quantum dots (CQDs) effectively combine the advantages of multiple photocatalytic materials, thereby enhancing degradation efficiency and enabling the comprehensive optimization of photocatalytic performance. An organic/inorganic ternary S-scheme system consisting of carbon quantum dots (CQDs), tetra(4-carboxyphenyl) porphyrin (TCPP), and BiOBr (BOB) microspheres (TCPP/CQDs/BOB) was ingeniously constructed [93]. In this design system, ternary or multicomposite systems utilizing carbon quantum dots as intermediates are created. These designs typically integrate organic and inorganic components smartly, creating a robust internal electric field at the interface. This configuration facilitates the swift transfer of photogenerated electrons, leading to the efficient degradation of TCs. This characteristic simplifies effective interface interaction with g-C$_3$N$_4$-based materials. Hu introduced a novel approach involving "in situ composites modified by chlorine-doped CQDs" [94]. In the metal-free g-C$_3$N$_4$-based photocatalyst system, carbon quantum dots facilitate in situ growth, while the doped nonmetals and g-C$_3$N$_4$ engage in an in situ coupling reaction. This interaction yields a conjugate that demonstrates enhanced photocatalytic degradation performance and hydrogen production efficiency, compared to the individual components.

Recent studies have focused on the green synthesis of CQDs using eco-friendly resources such as rice husk, lemon peel, coal tar pitch, peach juice, and sugarcane juice. Nayoon Choi et al. incorporated CQDs derived from citric acid and lemon juice into

TiO$_2$ nanocomposites, achieving a TC removal rate of 91.5% after 120 min of visible light irradiation [95]. Similarly, Ajaypal Kaur et al. used rice straw as a carbon precursor to synthesize CQDs for photocatalytic applications [96]. They prepared CQD nanocomposites with titanium-substituted and magnesium-substituted strontium ferrite nanoparticles (Sr$_{0.4}$Ti$_{0.4}$Mg$_{0.2}$Fe$_2$O$_{4.4}$) via ultrasonic treatment; the 2:1 ratio CQD-Sr$_{0.4}$Ti$_{0.4}$Mg$_{0.2}$Fe$_2$O$_{4.4}$ exhibited remarkable photocatalytic and antibacterial activity, with tetracycline hydrochloride degradation efficiencies between 97.1% and 99.0% under visible light. Table 4 provides a summary of recent studies conducted over the past two years on the degradation of TCs and TCH in aquatic environments using a carbon quantum dot photocatalyst.

Table 4. Degradation of TCs and TCH by carbon quantum dot photocatalyst.

Pollutants	Materials	Band-Gap Energy (eV)	Degradation Condition			Degradation Efficiency	Ref.
			Time/min	Catalyst Dosage	Concentration of Pollutants (mg/L)		
TCs	CQDs/Cu$_2$O	2.04	100	100 mg	10	92.49%	[97]
TCs	g-C$_3$N$_4$/CQD/Fe$_8$Ni$_2$BTC [a]	2.44	90	2500 mg/L	30	98.28%	[98]
TCs	Ag$_3$PO$_4$/g-C$_3$N$_4$/FeNi-BTC [a]/CQD	2.56	60	400 mg/L	30	98.4%	[99]
TCH	BiOBr/g-C$_3$N$_4$/CQDs	-	50	1000 mg/L	10	99.63%	[100]
TCs	NCDs/BiOBr/AgBr	-	60	40 mg	20	94%	[101]
TCs	P(1.0)-CQD/Ni-MOL(nickel metal-organic layer)	2.23	120	30mg	100	98.98%	[102]
TCs	CQDS/BiVO$_4$	-	30	500 mg/L	10	92.3%	[103]
TCs	N-CQDs/TiO$_2$	2.85	120	200 mg/L	10	97.7%	[104]
TCs	CQDs/FeOx	1.40	320	2000 mg/L	20	98.21%	[105]
TCH	CA (carbon aerogel)/BiOCl	3.16	120	200 mg/L	20	100%	[106]

[a] BTC, Benzene-1,3,5-tricarboxylic acid.

2.5. Floatation-Based Photocatalysts

Conventional photocatalysts are predominantly in powder form, and require constant stirring during use to prevent sedimentation in aqueous environments. As the water depth increases, the permissible light intensity markedly decreases, which adversely impacts photocatalytic efficiency and escalates energy production costs. In addition, conventional photocatalysts encounter challenges related to incomplete solid–liquid separation, complicating recovery processes. Therefore, floatable photocatalysts have emerged. The photocatalytic process operates at the water surface as illustrated in Figure 2, effectively capturing light without the risk of sinking. The robust interactions between floating carriers and surfactant-like nanoparticles enhance both reusability and stability. Floating photocatalysts can be categorized into two types: the support-type and self-floating photocatalysts. Support-type photocatalysts integrate a carrier with a catalyst to facilitate effective light absorption while ensuring stable flotation on the water's surface. In contrast, self-floating photocatalysts do not require an external carrier; they achieve buoyancy through the formation of numerous closed pores or hollow structures within their framework.

The operational environment requires high stability and continuous performance from photocatalyst carriers. Expanded perlite (EP), with its chemical stability, homogeneity, and large specific surface area, is an excellent support choice. The SiO$_2$ in the carrier forms strong Ti-O-Si bonds with TiO$_2$ and other active components. However, untreated expanded perlite's thin walls and fragility, coupled with high water absorption, can lead to delamination and reduced performance. Developing self-floating functional materials via in situ growth treatments enhances catalyst adhesion to the modified expanded perlite support, thereby improving stability and efficiency. Chen et al. developed a floating photocatalyst by utilizing melamine as the precursor for g-C$_3$N$_4$ and expanded perlite as the support [107]. Liu et al. developed a buoyant expanded perlite (EP) modified with hpolydopamine (PDA) as a carrier and used a room-temperature stirring method to grow MIL-88A (Fe) in situ on its surface, resulting in the large-scale production of floating MIL-88A (Fe)@EP (M@EP) photocatalysts [108]. In situ modification enhanced the loading rate

of the original photocatalysts, establishing a robust interface between the photocatalyst and expanded perlite.
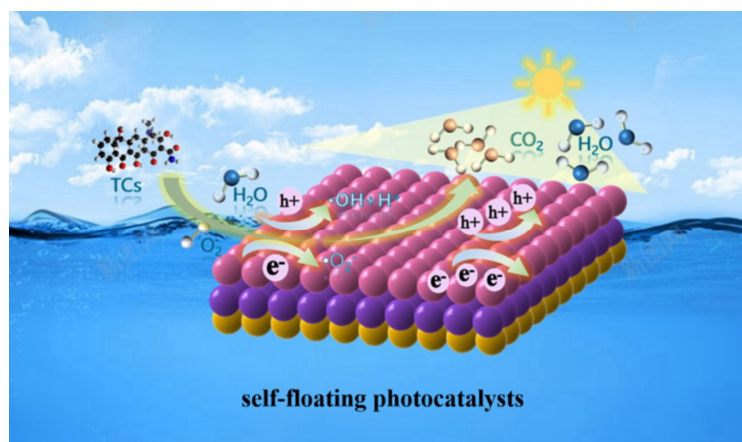

Figure 2. Mechanism of degradation of TCs by self-floating photocatalyst.

By developing self-floating photocatalysts, the effective capture probability of light in the photocatalytic redox cycle can be significantly enhanced. This advancement facilitates the oxidation of pollutants and the reduction of CO_2, leading to a marked increase in hydrogen evolution rates. Such findings offer valuable insights for designing cost-effective, clean, and efficient floating photocatalysts. Wang et al. integrated $ZnSnO_3$ quantum dots (ZSO QDs) into bismaleimide-co-vinylbenzene porous microspheres (PBMs) to create a polymer composite microreactor with an S-scheme heterojunction [109]. The antibiotic pollutants were efficiently subjected to catalytic oxidation and degradation under light exposure, resulting in the reduction of generated CO_2 to high-value carbon monoxide (CO). Zhang et al. developed a self-floating wood evaporator for photothermal evaporation and catalytic degradation by functionalizing lightwood with carbon nanotubes (CNTs) and manganese dioxide (MnO_2) nanoflowers using solar-thermal conversion materials [110]. The unique wetting properties of the dry lightwood substrate enable the formation of a non-wetting internal structure and precise water channels, ensuring effective water supply, thermal localization, sufficient mass transfer, and high buoyancy. Table 5 provides a summary of recent studies conducted over the past two years on the degradation of TCs and TCH in aquatic environments using floatation-based photocatalysts.

Table 5. Degradation of TCs and TCH by floatation-based photocatalysts.

Pollutants	Materials	Band-Gap Energy (eV)	Degradation Condition			Degradation Efficiency	Ref.
			Time/min	Catalyst Dosage	Concentration of Pollutants (mg/L)		
TCH	g-C_3N_4 on polyurethane foam	-	120	30 mg/L	5	96.8%	[111]
TCs	BiOCl/BiOBr@FACs (fly ash cenospheres)	2.98	60	1000 mg/L	30	86.1%	[112]
TCs	V-$BiOIO_3$/FTCN (fish-scale tubular carbon nitride)	-	60	400 mg/L	10	89%	[113]
TCs	CuO-MoS_2/C_3N_4-expanded graphite	-	60	330 mg/L	50	99%	[114]
TCs	Bi-$Bi_2O_2CO_3$-$ZnBi_2O_4$	3.05	180	875 mg/L	10	97.5%	[115]
TCH	Self-suspending aluminum-plastic supported TiO_2	-	240	2000 mg/L	30	93.6%	[116]
TCs	$FeMo_3O_x$/g-C_3N_4/EP (expanded perlite)	2.05	60	1330 mg/L	25	98%	[117]
TCH	FeOOH/EPE(expandable polyethylene)	-	14	350 mg	20	96.76%	[118]
TCs	PS@TiO_2/Bi_2O_3	3.53	60	200 mg/L	50	88.4%	[119]
TCs	$FeMo_3O_x$/C_3N_4-EP (expanded perlite)	-	30	1000 mg/L	50	97.8%	[120]

Future research may focus on integrating photocatalysis and electrophotocatalysis in this floating system to enhance treatment and monitoring capabilities for pharmaceutical wastewater. The floating photocatalyst absorbs solar energy from the water's surface to degrade organic pollutants, while electrocatalytic processes ensure complete mineraliza-

tion. Continuous monitoring of electrical current allows real-time assessment of chemical concentrations in the water, facilitating timely adjustments for optimization.

2.6. Heterojunction Photocatalysts

In photocatalytic reactions, light excites electrons in the valence band (VB) of a semiconductor photocatalyst, promoting them to the conduction band (CB) and generating electron–hole pairs. These pairs are then separated and migrate to the surface, where oxidation–reduction reactions occur. Finally, fractional charge carriers recombine at the interface [121]. Thus, effective light absorption is essential for enhancing photocatalytic efficiency.

To improve visible-light-responsive photocatalysts, it is crucial to accelerate the generation and transport of photogenerated charge carriers while delaying their recombination [122]. Single-component semiconductor photocatalysts often struggle to achieve both broad light absorption and efficient charge separation, leading to inadequate performance for practical applications [123]. Heterojunction photocatalysts offer a promising solution by combining the strengths of different components. They consist of interfaces between semiconductors with varying bandgap structures, and can be classified into four types: Type I, Type II, Z-type, and S-type heterojunctions and as shown in Figure 3 below.
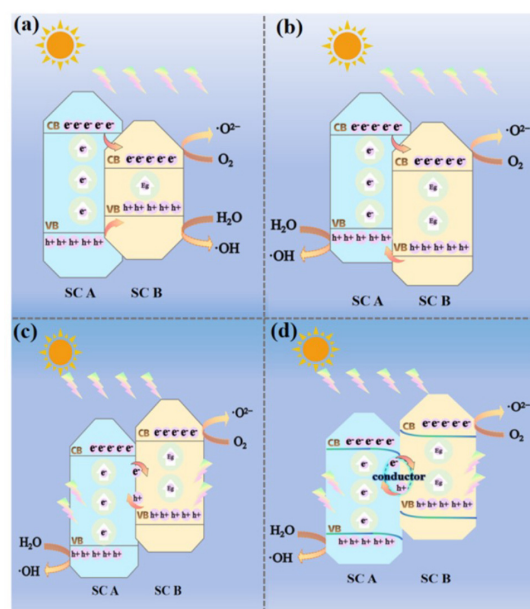

Figure 3. (**a**) Type-I heterojunction photocatalysts. (**b**) Type-II heterojunction photocatalysts. (**c**) Z-scheme heterojunction and (**d**) S-scheme heterojunction.

2.6.1. Type-I and Type-II Heterojunction Photocatalysts

In Type I heterojunction photocatalytic systems, the CB level of semiconductor A is higher than that of semiconductor B, while its VB position is lower [124]. This configuration leads to the accumulation of photo-generated charge carriers in the VB and CB of semiconductor B under illumination, resulting in ineffective electron–hole separation and a high recombination rate, which impairs photocatalytic efficiency. Type II heterojunction photocatalysts were developed to overcome this limitation. In these systems, both the VB and CB levels of semiconductor A are above those of semiconductor B. When illuminated with light equal to or greater than the bandgap energy of semiconductor B, electrons are excited into the empty CB, while leaving holes in the VB. The holes migrate to semiconductor A as photo-generated electrons move toward semiconductor B. This simultaneous migration reduces recombination rates and extends electron lifetimes, thereby enhancing photocatalytic efficiency. Among Type II heterojunctions, the p-n heterojunction demonstrates the most enhanced performance. Under illumination, both P-type and N-type materials are photoex-

cited, generating charge carriers. When these semiconductors come into close contact, an internal electric field forms at the interface due to the difference in their Fermi energy (EF) levels. This leads to the migration of electrons from the P-type to the N-type semiconductor, effectively separating the electron–hole pairs and thereby improving the photocatalytic activity of the material [125]. A p-n heterojunction, NiFeO/ZnInS was synthesized by Wang et al. to enhance carrier migration [126]. Yu et al. synthesized copper oxide/calcium tungsten oxide (CuO/CaWO) composites via a straightforward hydrothermal method [127]. The formation of the p-n heterojunction facilitates the generation of holes and electrons at the interface between two distinct semiconductor catalytic materials, resulting in the establishment of a built-in electric field within the composite catalyst. This configuration exhibits enhanced electroactivity compared to individual semiconductor catalysts, thereby accelerating the disintegration of TCs.

2.6.2. Z-Scheme Heterojunction Photocatalysts

The Z-type heterojunction facilitates the recombination of electrons and holes generated in two low-energy semiconductors. It first combines holes with lower oxidation-reduction potential from semiconductors A and B with electrons, while retaining those with higher potentials [128]. Photogenerated holes accumulate at the VB of SC-A and electrons at the CB of SC-B, enabling distinct oxidation and reduction reactions within this system. This structure effectively enhances electron–hole pair separation while preserving the catalyst's strong oxidizing and reducing capabilities.

However, this system has limitations. Traditional Z-scheme photocatalysts require liquid phases, and most liquid-phase redox media are unstable and prone to deactivation, which reduces photocatalytic efficiency. Therefore, materials with good electrical conductivity are essential. Otherwise, electron transfer pathways may be hindered, halting the photocatalytic reaction.

Noble metals are excellent electronic mediators in solid-state Z-type photocatalysts. Ma et al. synthesized a hierarchical flower-like Z-type heterojunction using microwave-assisted methods with metallic silver as a charge transfer bridge [129]. The optimized photocatalyst exhibited impressive photocatalytic performance under visible light, significantly surpassing the efficacy of pure Ag/AgBr. In parallel, Lu et al. successfully fabricated an AgI/PCN-224 (APN-x composite material) Z-type heterojunction via in situ precipitation [130]. However, the use of noble metals as co-catalysts not only has a limited scope of application, but also increases the cost of the catalyst. To overcome the limitations of heterojunction morphology, it is crucial to develop a more universal approach for the future. This advancement will facilitate the creation of non-noble metal catalysts for CO_2 reduction and H_2O oxidation, thereby enhancing spatial separation on semiconductor surfaces and promoting efficient photocatalytic degradation of TCs.

Moreover, coupling Z-scheme photocatalysts with other types of photocatalysts represents an effective strategy for optimizing photocatalytic performance [131]. A novel $CuAl_2O_4/MoS_2/BaFe_{12}O_{19}$ (CAO/MS/BFO) magnetic photocatalyst was designed to couple both Type I and Z-scheme heterojunctions [132]. Zhou et al. prepared a novel Z-type + II-type ternary heterojunction nanocomposite by one-step solvothermal method using g-C_3N_4, FeS and FeO as raw materials. The enhanced light-absorption capacity, spatially efficient carrier separation, and increased electron transfer pathways within the Z-Scheme + Type II composite system significantly contributed to the improved photocatalytic degradation efficiency. Degradation efficiency under optimal conditions is almost three times higher than pure g-C_3N_4 [133]. In the long run, the photocatalytic fuel cell (PFC) system represents a novel approach for environmental remediation, leveraging the unique benefits of composite photocatalysts that integrate diverse heterojunction structures. By strategically positioning each component on appropriate electrodes and systematically optimizing the energy band alignment between the cathode and anode, this system enhances electron transfer between electrodes. This arrangement not only boosts the synergistic photocatalytic effects of both electrodes, but also significantly improves the degradation efficiency of TCs.

2.6.3. S-Scheme Heterojunction Photocatalysts

Currently, the majority of photocatalysts are limited to utilizing ultraviolet (UV) and visible light for photocatalytic reactions, often overlooking the potential of near-infrared (NIR) radiation. NIR constitutes over 50% of solar radiation, but has been largely disregarded due to its lower photon energy. Nevertheless, NIR can enhance the temperature of the reaction system through photothermal effects, thereby facilitating photocatalytic processes [134].

The effective utilization of near-infrared light to enhance solar energy-conversion efficiency and photocatalytic performance is of significant importance. The S-type heterojunction has emerged as a promising solution, by improving the separation efficiency of photogenerated charge carriers and enhancing the redox capabilities of electrons (e^-) and holes (h^+). This S-type heterojunction comprises a reduction photocatalyst (RP) with a higher CB level and Fermi level, alongside an oxidation photocatalyst (OP) characterized by a lower VB level and Fermi level. Upon contact, electrons migrate from RP to OP due to the difference in their Fermi levels, resulting in the formation of an internal electric field (IEF) at their interface that induces band bending. This IEF effectively prevents the recombination of photogenerated electrons in the conduction band of OP with holes in the valence band of RP, while retaining strong redox-active charge carriers. Additionally, incorporating narrower-bandgap semiconductors can broaden the light absorption range while maintaining efficient charge separation, thus enhancing photocatalytic efficiency.

Due to these advantages, S-type heterojunctions have been widely applied in various photocatalytic processes [135]. A robust MnFeO/ZIF-8 S-scheme heterojunction was synthesized using an eco-friendly green approach [136]. Additionally, hydroxyl ($\cdot$OH) radicals were identified as the primary oxidants driving the photocatalytic degradation process. Wang et al. developed an innovative S-type heterojunction composed of biochar/g-C_3N_4/BiOBr (BCN/BiOBr) [137], which demonstrated efficient tetracycline degradation. Moreover, the S-type heterojunction is an outstanding option for photoanodes in emerging photoelectrochemical technologies, such as the Fenton process combined with photocatalysis. This configuration facilitates effective separation of electron–hole pairs, enhancing the redox capacity through mechanisms involving internal electric fields, band edge bending, and Coulomb interactions. For instance, Sun et al. developed a photoelectrocatalytic system featuring an S-type MgO/g-C_3N_4 photoanode paired with a modified carbon felt (MCF) cathode [138]. This heterojunction, composed of both organic and inorganic semiconductors, maximizes the benefits of each material, expanding light absorption and mitigating the rapid recombination of photogenerated electron–hole pairs typical of single semiconductor systems. Additionally, the nonmetallic semiconductor serves as an electron donor, thereby reducing the leaching of toxic metal ions. Table 6 shows their recent applications for degrading pesticides and pharmaceutical pollutants over the past two years.

Table 6. Degradation of TCs and TCH by S-Scheme heterojunction photocatalysts.

Pollutants	Materials	Band-Gap Magnitude			Degradation Conditions			Degradation Efficiency	Ref.
		Semiconductor (eV)		Heterojunction (eV)	Time (min)	Catalyst Dosage	Pollutant Concentration (mg/L)		
		A	B						
TCs	In_2O_3/TiO_2	2.84	3.2	2.48	180	500 mg/L	20	98%	[139]
Oxytetracycline (OTC)	CdMoO4/CdO	3.6	2.1	-	90	50 mg	40	95.38%	[140]
TCs	$ZnO/Zn_3(PO_4)_2$	3.23	3.03	3.10	90	50 mg	20	97%	[141]
TCH	SnS_2/TiO_2	2.21	3.00	2.73	90	1.5 cm^2	10	93.4%	[142]
TCs	$InVO_4/ZnIn_2S_4$	2.00	2.30	-	45	600 mg/L	50	90.69%	[143]
TCs	$(BiO)_2CO_3/BiOCl$	3.02	3.17	3.05	60	50 mg	10	95.3%	[144]
TCs	$g-C_3N_4/Mn_{1.1}Fe_{1.9}O_4$	2.75	2.03	-	90	500 mg/L	40	94.7%	[145]
TCs	$Bi_4O_5I_2/Bi_{3.64}Mo_{0.36}O_{6.55}$	2.27	2.41	-	60	200 mg/L	10	91%	[146]
TCH	$In_2O_3/Bi_4O_5Br_2$	2.63	2.57	-	100	35 mg	20	92.4%	[147]
TCs	$Cu-MOF/ZnWO_4$	2.7	3.0	1.25	60	20 mg	20	98%	[148]

3. Catalytic Oxidation of Tetracycline Antibiotics by Photocatalytic Materials and Their Derivatives

3.1. Mechanism of Catalytic Oxidation of Tetracycline Antibiotics

The main mechanism of antibiotic photocatalytic degradation can be summarized as the generation of active species (H^+, $\cdot O^{2-}$, $\cdot OH$) and the degradation of antibiotic TCs [149]. The specific photocatalytic mechanism is shown in the Figure 4 below. The process is often accompanied by the simultaneous occurrence of oxidation and reduction reactions. Specifically, when photons with energy greater than the bandgap of the photocatalyst strike its surface, electrons in the valence band (VB) are excited to the conduction band (CB), generating an equal number of positively charged holes (h^+) in the VB (Equation (1)). These holes migrate to the surface, and if the standard oxidation–reduction potential exceeds +1.99 eV ($E_0(\cdot OH/OH^-)$) and 2.27 eV ($E_0(H_2O/\cdot OH)$) [150], h^+ can be captured by H_2O, producing highly oxidative $\cdot OH$ radicals. Additionally, depending on medium pH (Equation (2)), hydroxyl radicals ($\cdot OH$) are generated during H_2O/OH^- oxidation [151]. Both OH^- and $\cdot OH$ serve as highly reactive oxidants in photocatalytic processes.
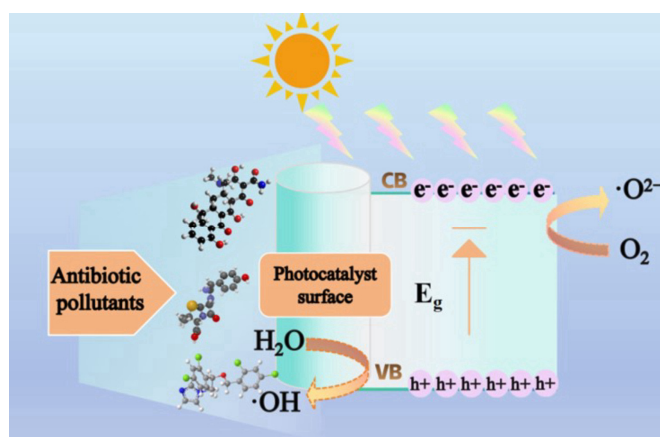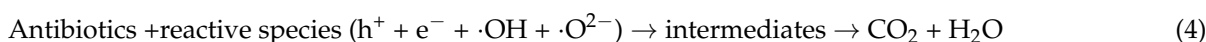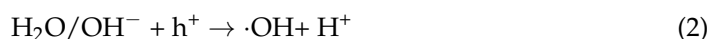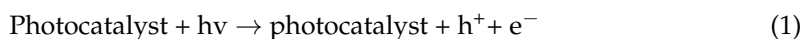

Figure 4. Mechanism of catalytic oxidation of antibiotics.

When the standard oxidation–reduction potential of CB is below -0.33 eV ($E_0(O_2/\cdot O^{2-})$ = -0.33 eV) [150], photo-excited electrons migrating to the semiconductor surface typically react with adsorbed O_2, generating free radicals such as superoxide anion $\cdot O^{2-}$ (Equation (3)). These radicals, including OH^- and $\cdot OH$, can then migrate to the catalyst surface and engage in oxidation–reduction reactions with antibiotics, promoting the degradation of tetracyclines (TCs) [152] (Equation (4)).

$$\text{Photocatalyst} + h\nu \rightarrow \text{photocatalyst} + h^+ + e^- \tag{1}$$

$$H_2O/OH^- + h^+ \rightarrow \cdot OH + H^+ \tag{2}$$

$$e^- + O_2 \rightarrow \cdot O^{2-} \tag{3}$$

$$\text{Antibiotics} + \text{reactive species} (h^+ + e^- + \cdot OH + \cdot O^{2-}) \rightarrow \text{intermediates} \rightarrow CO_2 + H_2O \tag{4}$$

However, photocatalytic processes typically necessitate continuous external light illumination to drive photoredox reactions, which significantly limits their applicability in dark environments. And it is crucial to study the mechanism of TCs degradation under unnatural light conditions [153].

Under UV light irradiation, heterojunction photocatalysts typically generate an intrinsic electric field at the interface between semiconductors. Wei et al. investigated the tetracycline degradation efficiency of oxygen-doped g-C_3N_4/BiOCl (S-scheme) heterojunctions under UV light [154]. Density functional theory (DFT) calculations and ultraviolet photoelectron spectroscopy (UPS) jointly revealed a unique chemical environment and electronic structure between OCN and BiOCl, formed due to the built-in electric field,

which facilitated enhanced charge migration for photogenerated currents. Xu et al. successfully synthesized BiOCl/OVs–$BiPO_4$ heterojunction photocatalysts in situ by treating $BiPO_4$ with dilute hydrochloric acid (HCl) under hydrothermal conditions [155]. Systematic characterization showed that the surface oxygen vacancies (OVs) and the interface electric field at the heterojunction accelerated the separation and migration of photogenerated carriers, while the surface OVs provided more active sites for adsorption and reaction. Wang et al. prepared a series of highly active and stable visible-light-responsive photocatalysts via solvothermal methods [156]. UV photoelectron spectroscopy (UPS), X-ray photoelectron spectroscopy (XPS), and electron spin resonance (ESR) measurements confirmed the formation of a Z-scheme heterojunction between $NiIn_2S_4$ and UiO-66. The synergistic effects of the built-in electric field, energy band bending, and Coulomb interactions at the Z-scheme interface facilitated the suppression of photogenerated electron–hole recombination, significantly enhancing photocatalytic activity.

However, the photocatalytic mechanisms vary, depending on the material's efficiency in utilizing light. An ideal photocatalyst should simultaneously maintain broad light absorption across the solar radiation spectrum (requiring a narrow bandgap) and strong redox capability (requiring a wide bandgap). Common wide-bandgap semiconductors typically absorb light within the UV region, where UV light with wavelengths shorter than 420 nm accounts for only about 4% of solar energy. Therefore, investigating the optimal degradation mechanism of efficient wide-bandgap photocatalysts under UV light and the efficient utilization of broad-spectrum light for tetracycline degradation by narrow-bandgap photocatalysts becomes particularly important [157]. Zhao et al. overcame the weak UV response issue caused by the wide bandgap of $Bi_2O_2CO_3$ by surface modification with g-C_3N_4, which improved its photocatalytic activity [158]. Transient photocurrent measurements revealed an increase in photogenerated carriers, and photoluminescence (PL) spectra indicated that surface modification with g-C_3N_4 suppressed the recombination of photogenerated electrons and holes, significantly improving carrier separation efficiency. Zhou et al. synthesized nitrogen-deficient g-C_3N_4 using formic acid-assisted pyrolysis, with formic acid used to modify the top atoms and effectively reduce the bandgap [159]. Photochemical experiments confirmed that $\cdot O_2^-$ and $^1O_2$ free radicals dominated the photocatalytic degradation process.

Moreover, photocatalytic processes require continuous external light illumination to drive photoredox reactions, which severely hinders their application in dark environments. In the absence of light at night, photocatalytic systems based on free radicals for the degradation of refractory organic pollutants in aquatic environments tend to enter a dormant state. Therefore, A 24 h photocatalyst, CCN@SMSED, was synthesized through the in situ growth of cyanide-deficient g-C_3N_4 on $Sr_2MgSi_2O_7$:Eu^{2+}, Dy^{3+} using a simple calcination method [160]. The generated free radicals ($\cdot O_2^-$ and $\cdot OH$) and non-free radicals (h^+ and $^1O_2$) are key factors for the photocatalyst's excellent degradation of tetracycline under both light and dark conditions. The main degradation pathways for TCs include demethylation, ring-opening, deamination, and dehydration. Fu et al. synthesized Ti_3C_2/TiO_2/Ag persistent photocatalysts and further improved the dark reactivity using peroxomonosulfate (PMS) [161]. Shi et al. reported the synthesis of honeycombed S-doped g-CN-NiCoO catalysts via a one-step in situ growth method. These catalysts activated peroxymonosulfate (PMS), facilitating rapid degradation of high-concentration pollutants in both light and dark conditions [162]. In summary, materials that enable continuous photocatalytic degradation of TCs exhibit remarkable electron storage capacity, allowing them to retain additional excitation charges while generating photogenerated electron–hole pairs under light irradiation. This stored charge can subsequently be released to facilitate sustained catalytic oxidation during dark reactions after light exposure, thereby ensuring uninterrupted photocatalytic activity throughout the day.

3.2. Strategies for Optimising Photocatalyst Degradation of Tetracycline Antibiotics

3.2.1. Separation and Charge Transfer Rates of Catalyst Surface Carriers

For most semiconductor photocatalysts, the recombination rate of surface-generated electron–hole pairs is very fast (10^{-12} to 10^{-11} s), while interfacial charge transfer occurs more slowly (10^{-7} to 10^{-9} s). Thus, charge capture, transfer, and surface reactions are crucial steps that determine the rate of photocatalytic degradation [163]. Inhibiting surface charge recombination and facilitating charge transfer to active sites are effective strategies for enhancing charge carrier dynamics and improving photocatalytic hydrogen production efficiency. Ma et al. synthesized ultra-thin $BiVO_4$ nanoplates (4–5 nm), providing abundant active sites for photocatalytic reactions and reducing the migration distance of photogenerated charge carriers [164]. By growing Au nanoparticles and Cu_2O nanolayers in situ on $BiVO_4$, multiple charge transport pathways were created, enhancing carrier separation and transport efficiency, which improved tetracycline degradation performance. The $BiVO_4$-Au-Cu_2O nanoplates exhibited superior catalytic activity (degradation rates were 4.3 times higher than $BiVO_4$ alone), as well as 1.6 and 2.3 times higher than those observed for $BiVO_4$-Au and $BiVO_4$-Cu_2O ultra-thin nanoplates, respectively. The localized surface plasmon resonance (LSPR) effect from Au nanoparticles also contributed to this enhancement. Capture experiments and electron paramagnetic resonance (EPR) confirmed that holes (h^+) and hydroxyl radicals ($\cdot$OH) were the main active species during photocatalysis.

The built-in electric field (IEF) plays a crucial role in semiconductor heterojunctions, serving not only as an intrinsic driving force that enhances the efficiency of charge carrier separation but also inducing the diffusion and migration of charge carriers at the interface between the catalyst and its substrate. Currently, most research on IEF provides only qualitative evidence for its existence; however, our understanding of its various distribution forms—from the interface to the molecular scale—including independent, series, and parallel configurations, as well as how geometric shape and arrangement influence charge carrier transport and interactions, remains limited. Chen et al. demonstrated that the anisotropic built-in electric fields induced by different crystal facets serve as an effective driving force for charge separation in photocatalytic materials [165]. By manipulating the anisotropy of exposed surfaces—referred to as "surface engineering strategies"—the efficiency of charge separation can be enhanced, facilitating spatial segregation of electrons and holes across distinct facets of the photocatalyst particles. Fermi-level calculations indicated that these $Co_{1-x}S$ nanosheets function as electron "pumps," enabling spontaneous charge transfer to multiple Co_3O_4 nanowires and establishing a multi-parallel built-in electric field (MPBIEF). This electric field is distributed parallel to the plane of $Co_{1-x}S$, leading to an asymmetric distribution of surface charges at the interface with Co_3O_4, thereby creating localized "electron reservoirs." Such a distinctive architecture promotes directed asymmetric diffusion motion of charge carriers under illumination conditions, ultimately achieving efficient separation and migration of these carriers.

3.2.2. Broad-Spectrum Response Characteristics

In the context of photocatalysis, a fundamental contradiction exists between strong redox capabilities and broad spectral responsiveness. For wide-bandgap photocatalysts, achieving robust reduction or oxidation abilities inevitably results in light absorption limitations, which consequently diminish their photocatalytic activity. Therefore, it is crucial to ingeniously design the light absorption intensity of these photocatalysts while maintaining their inherent strong redox properties [166]. Recently, monomers featuring triazine structures, porphyrins or phenolic functional groups such as 2,4,6-trimethoxybenzoquinone have been employed in the synthesis of covalent organic frameworks (COFs) to enhance charge separation efficiency. However, the majority of COFs exhibit a narrow absorption range, typically between 200 nm and 550 nm, which results in reduced photocatalytic efficiency. Fang et al. selected Py(1,3,6,8-tetrakis(4-aminophenyl)pyrene) molecules with conjugated electrons as the electron donor units and TpDPP(5,5′-(2,5-bis(2-ethylhexyl)−3,6-dioxo-2,3,5,6-tetrahydropyrrolo [3,4-c]pyrrole-1,4-diyl)bis(thiophene-2-carbaldehyde) as

the electron acceptor, to synthesize novel TpDPP-Py COFs featuring a large π-conjugated system [167]. They observed that thiophene functional groups were precisely incorporated into the electron acceptor units of the TpDPP-Py COFs, which not only significantly extended the spectral absorption range from 200 nm to 900 nm (covering ultraviolet, visible, and near-infrared light) but also imparted dual-photon and triple-photon absorption effects, thereby greatly enhancing sunlight utilization efficiency.

In addition to requiring a narrow bandgap for effective solar light absorption, the thermodynamic criteria for water splitting demand precise alignment of the conduction and valence bands. This alignment is essential to ensure that photon-generated charge carriers possess sufficient energy to drive subsequent catalytic reactions, particularly given the significant overpotential associated with water oxidation. Currently reported photocatalysts absorbing wavelengths above 600 nm are primarily non-metal-doped materials, such as nitrogen (N) and sulfur (S), which are prone to self-corrosion from oxidation by photo-generated holes under illumination. Thus, designing novel oxide semiconductor materials with broad-spectrum absorption and structural stability presents considerable challenges in this field. Tao et al. examined the outer electronic structure of bismuth in bismuth-based semiconductors, focusing on the influence of crystal structure and orbital hybridization on band modulation [168]. They investigated bismuth chromate materials with varied chemical compositions and crystal structures. Through optimized synthesis conditions, they synthesized a novel triclinic phase of bismuth chromate (Bi_2CrO_6). Optical absorption studies indicated that the bandwidth of triclinic Bi_2CrO_6 is approximately 1.86 eV, with an absorption edge exceeding 650 nm; additionally, the valence band position meets thermodynamic criteria for both proton reduction and water oxidation. Zhou et al. synthesized InGaN/GaN nanowires (NWs) on silicon substrates using molecular-beam epitaxy (MBE), and subsequently loaded Rh/Cr_2O_3 core/shell and Co_3O_4 nanoparticles as co-photocatalysts via in situ photodeposition [169]. The results indicate that the InGaN/GaN NWs exhibit high crystallinity, growing along the [002] direction, with GaN serving as a capping layer to support the InGaN structure. The distribution of indium within the InGaN/GaN NWs induces variations in the bandgap, thereby facilitating broadband light absorption.

3.2.3. Efficient Activation of Persulfates

AOPs based on persulfates, including peroxymonosulfate (PMS) and peroxydisulfate (PDS), are effective for degrading organic pollutants. These compounds possess strong oxidizing abilities (E_0 of 1.96 V for PDS and 1.75 V for PMS), a wide pH range, favorable selectivity, and long half-lives, making them attractive alternatives in water treatment and soil remediation. However, PMS and PDS typically require activation to generate free radicals or reactive oxygen species (ROS) for effective pollutant degradation. Carbon nanotubes (CNTs) have shown excellent performance in activating persulfates as versatile carbon nanomaterials [170–172].

Zhao et al. developed a copper doping strategy that enhances the dispersion of B-O-Cu sites and graphitic nitrogen in boron and nitrogen co-doped carbon nanotubes, facilitating the activation of peroxymonosulfate (PMS) for TC degradation [173]. The substantial improvement in degradation efficiency is attributed to B-O-Cu sites promoting Cu(I)/Cu(II) redox cycling and graphitic nitrogen enhancing electron transfer with PMS. Additionally, transition-metal photocatalysts like Cu, Ag, Co, Mn, and Fe are effective in activating PMS to generate sulfate radicals (SO_4^{2-}). Chen et al. synthesized a novel Fe-Mn bimetallic catalyst using Mn-doped α-Fe_2O_3 precursors via a one-step hydrothermal method, activating persulfate (PMS) for TC degradation [174]. Density-of-states analysis revealed that the electronic spin characteristics of FMDS-3 brought its peak closer to the Fermi level, promoting PMS adsorption on the catalyst surface.

Metal-free g-C_3N_4 effectively integrates photocatalytic technology with persulfate (PS) activation, creating a complementary advanced oxidation process. This environmentally friendly and chemically stable material is promising for PS activation under light. However,

its inherent limitations render it nearly inactive in the dark. Thus, there is significant interest in enhancing the oxidative degradation efficiency of this system while reducing energy consumption, by developing dual-function metal-free g-C_3N_4 photocatalysts that can activate PS both photochemically and non-photochemically. Tan et al. [175] enhanced g-C_3N_4 through oxygen doping, significantly improving its non-photochemical and photocatalytic activation capabilities. This was achieved by optimizing the electronic structure of oxygen-doped g-C_3N_4(OCN), increasing PMS adsorption capacity, enhancing light capture ability, and lowering the energy barrier for PMS activation. Density functional theory (DFT) calculations revealed that PMS exhibited higher adsorption energy and Bader charge on OCN compared to g-C_3N_4, indicating that it is more easily adsorbed, dissociated, and activated on OCN.

4. Novel Technologies Under Development

4.1. Novel Composite Structures of Photocatalysts

4.1.1. Aerogel-Based Photocatalysts

Aerogels are three-dimensional nanoparticle-assembled materials characterized by low density, high porosity, and a large specific-surface area. These properties confer significant application potential in areas such as thermal insulation, photocatalysis, and drug delivery. With advancements in synthesis techniques, the role of aerogel materials in photocatalysis has evolved from initial physical adsorption to encompass applications in environmental remediation and photochemical reactions related to clean energy [176].

Yuan [176] utilized the sol–gel method with titanium tetraisopropoxide and zinc acetate to prepare $Zn_2Ti_3O_8$ aerogel precursors via CO_2 supercritical drying. By adjusting the heat-treatment temperature, they synthesized $Zn_2Ti_3O_8$ aerogel photocatalysts. Qiu et al. synthesized a novel lightweight multifunctional C/TiO_2@rGO aerogel via one-step in situ oxidation of MXene [177]. Its unique three-dimensional porous structure and precise component regulation result in an exceptionally low density, excellent electromagnetic wave attenuation and favorable impedance matching. Zhang et al. obtained delignified wood aerogels (DWAs) from natural wood (NW) by the acetic acid–hydrogen peroxide method using poplar wood as raw material, and further produced aldolylated wood aerogels (DAWAs) with satisfactory porosity, high specific-surface area and abundant aldehyde functional groups [178]. In summary, the porous structure of aerogels enhances the physical adsorption and transport of tetracycline molecules, optimizing the utilization of photogenerated charge carriers. The high specific-surface area of aerogels provides abundant active sites, significantly improving photocatalytic degradation efficiency. Notably, aerogels with unique three-dimensional porous structures possess more precise component regulation systems, resulting in extremely low density, excellent electromagnetic wave attenuation, and good impedance matching.

4.1.2. Hollow Spherical-Shell Photocatalysts

Hollow nanostructures offer a number of advantages over conventional bulk materials in photocatalyst design, including effective light scattering and absorption, shortening of charge migration distances and the enabling of directional charge separation, and the provision of a large number of reaction sites on the shell surface [179]. Liu et al. synthesized g-C_3N_4/MoS_2-V-3 (CN/MS-V-3) exhibiting remarkable photocatalytic efficiency, by integrating g-C_3N_4 with a hollow structured MoS_2 (MoS_2-V) [180]. This combination significantly enhanced visible light absorption and carrier separation efficiency, thereby promoting the photocatalytic degradation of TCs. Additionally, Cu^{2+} ions adsorbed on the surface of CN/MS-V-3 were reduced to Cu^+ within the photocatalytic system, facilitating increased carrier migration and enhancing reactive oxygen species (ROS) generation through the transfer processes involving Cu^{2+}/Cu^+ and Mo^{4+}/Mo^{6+}. Notably, this design ingeniously leverages the electron transport characteristics of co-existing heavy metals, presenting an effective strategy for addressing co-contamination issues arising from antibiotics and heavy metals.

Despite the impressive capabilities of photocatalytic systems, there is a notable gap in developing high-oxidation materials for persistent pollutant remediation. Tin oxide (SnO) has a higher oxidation potential than titanium dioxide (TiO_2) and shows better stability under complex environmental conditions, making it a promising candidate. However, its wide bandgap limits its photocatalytic activity, preventing it from fully realizing its potential. Luo et al. modified copper-doped tin oxide hollow spheres derived from egg yolk shells (YS-(5)CSO) using a metal-glycolate-assisted metal–organic framework, creating a multi-layered structure with a large surface area [181]. This design enhances photon capture through multiple re-expansion/scattering effects and improves charge dissociation by minimizing ion diffusion pathways. The YS-(5)CSO shell was then combined with MnCoO nanoparticles (Np-MCO@YS-(5)CSO) to form an S-type heterojunction.

Specially structured photocatalysts can enhance reactive sites and improve the separation of photogenerated electron–hole pairs. Wu et al. developed a novel Ag_2S/Bi_4NbO_8Cl photocatalyst via electrostatic interactions under ammonia conditions [182]. This catalyst features a "cookie"-like morphology with a strong interface, forming a Type II heterojunction that prevents photo-induced recombination. Electrons migrate from Ag_2S to Bi_4NbO_8Cl, avoiding the reduction of Ag^+ to metallic silver and stabilizing the catalyst. Sun et al. synthesized $Bi_{25}CoO_{40}$ silicate nanoplates with a thickness of approximately 1.4 nm, demonstrating sunlight spectrum absorption exceeding 900 nm [183]. The prominent exposure of the (400) plane creates a strong internal electric field that enhances charge separation and balances the generation of holes and superoxide radicals. The optimized morphology increases surface area for redox reactions and light harvesting, improving photodegradation performance for pollutants. Li et al. synthesized an iron photocatalyst using a coordination iron metal–organic framework precursor [184]. This method produced a bird's nest-structured photocatalyst composed of stacked nanoplatelets, increasing the surface area by 3.6 times. The FMO-NSs also included smaller nanoparticles and quantum dot satellites, enhancing charge separation. Photodegradation rates for TCH and oxytetracycline hydrochloride (OTCH) exceeded 90%, with most pollutants fully mineralized and demonstrating excellent reusability.

4.2. Novel Synthetic Methods of Photocatalysts

4.2.1. Molecularly Imprinted Photocatalysts

In recent years, researchers have focused on developing multifunctional materials for degrading persistent pollutants [185]. The demand for improved degradation efficiency in advanced oxidation processes (AOPs) has spurred interest in targeted catalytic materials made through molecular imprinting technology (MIP). The surface molecular imprinting (SMIP) process involves three steps: (1) forming non-covalent interactions between the target pollutant and functional monomers; (2) generating free radicals to polymerize crosslinkers, creating a selective imprinted layer on the catalyst; and (3) binding this layer to substrates, resulting in a novel catalyst with specific affinity for pollutants. These photocatalysts can effectively target and degrade persistent pollutants in water treatment by enriching them and activating free radicals for efficient degradation [186]. Lu et al. developed an imprinted non-metal S-type heterojunction photocatalytic membrane (IM-NSH-PM) using imprinting modification and dopamine adhesion methods [187]. This membrane demonstrated a high flux of 2548.6 L $m^{-2}h^{-1}bar^{-1}$, excellent self-cleaning properties, and remarkable stability. The imprinting process created cavities that matched TC's three-dimensional structure, enhancing its selective adsorption and degradation.

The ·OH radicals produced by photocatalytic reactions lack selectivity for specific target molecules, allowing them to attack organic material in wastewater. In real systems, where target pollutants coexist with high concentrations of low-toxicity substances, photocatalysts tend to remove higher concentrations, due to this lack of precision. Therefore, there is an urgent need for a photocatalyst that can selectively recognize and degrade target molecules. Fu et al. synthesized a TC-imprinted photocatalyst (TMIP) by a surface molecular-imprinting technique using NH-MIL-101 (Fe) as a carrier [188]. The TMIP

showed higher selectivity and adsorption capacity for TCs, with an adsorption capacity of up to 57.5 mg/g. Li et al. prepared 3D/1D magnetic molecularly imprinted fiber $Fe_3O_4@TiO_2/TC-TiO_2/SiO_2$ photocatalysts by electrostatic spinning with a large specific-surface area of 132.4 m^2/g [189]. The prepared photocatalysts exhibited a high selectivity coefficient of α = 737.38, and 100% removal of TCs was achieved in only 20 min. Based on the existing molecularly imprinted photocatalyst fabrication process, more molecularly imprinted-based photocatalysts with targeted high-degradation efficiency can be further explored in the future.

4.2.2. Biomimetic Photocatalysts

Structural control and defect engineering effectively enhance photocatalyst performance. Designing biomimetic structures that mimic natural biological architectures is a promising approach to further improve efficiency. This involves using unique biological entities—such as plant cells, tissues, microorganisms, and small molecules—as templates for synthesizing photocatalytic materials. By combining the features of these biological systems with semiconductor properties, the resulting biomimetic materials achieve enhanced structures, increased surface area, and higher porosity, leading to greater contact areas and active sites that significantly boost photocatalytic performance. Yuan et al. drew inspiration from the surface structures of natural leaves and plant transpiration to develop a gel film composed of copper alginate, carbon nanotubes, and copper sulfide–graphene oxide [190]. This photo-driven gel film exhibits specific adsorption properties for water evaporation, utilizing solar energy to facilitate the evaporation of water from contaminated surface sources, thereby enabling the extraction of tetracycline antibiotics for detection purposes. When integrated with a biomimetic adsorption detection chip designed for this application, it allows for in situ monitoring of tetracycline antibiotics in aquatic environments. Inspired by natural photosynthesis, Liu et al. synthesized a novel Z-type heterojunction photocatalyst, BiOBr/RGO/TCPP, by mimicking the multifunctional components of chloroplasts and the layered interconnected heterostructures [191]. The inbuilt electric field in the layered structure of BiOBr and interconnected RGO nanosheets formed a multi-channel electron and energy-transport chain. The final removal efficiency reached about 90%. Miquel Ortiz et al. developed efficient onion-shaped photocatalysts using pollen as a core template via a scalable electrochemical method, maintaining the structural integrity of sunflower pollen. The resulting multilayer structure increased surface area, enhancing light harvesting and pollutant adsorption [192]. Spent photocatalysts could be recovered as biological particles from pollen, meeting biofuel standards for low ash (<7%), low moisture (<8%), and high calorific value ($\approx$22.1 $\pm$ 0.3 MJ kg^{-1}). This indicates strong potential for green recycling applications. Future research may focus on advanced biomimetic photocatalysts and extending templating methods to synthesize metal–organic frameworks (MOFs) and carbon aerogels from biomass-derived sources.

5. Conclusions and Prospects

This paper presents a comprehensive review of the photocatalytic degradation of tetracycline antibiotics. It provides a detailed classification and overview of currently popular novel photocatalytic materials. Based on the seven types of photocatalytic materials synthesized as reviewed in the paper, including MOFs, metal- and nonmetal-doped, mesoporous material-loaded, carbon quantum dot modified, floatation-based, and heterojunction photocatalysts, these photocatalysts exhibit characteristics such as abundant active sites, broad light-absorption ranges, high efficiency in photogenerated carrier separation, and strong redox capabilities. The degradation mechanism of tetracycline antibiotics by these photocatalysts is elucidated. Additionally, an analytical discussion is provided regarding three critical factors that influence both the degradation efficiency and performance of the photocatalysts. Finally, recent advancements in new types of photocatalyst materials and innovative synthesis methods are selectively presented. A comparative analysis of the

tetracycline degradation performance of the photocatalytic materials mentioned in Table 7 was conducted.

Table 7. A comparative analysis of the TC degradation performance of the photocatalytic materials.

Types	Light Source	Preparation Method	Initial TC Concentration (mg/L)	Degradation Efficiency (%)	Reaction Time (min)	Side Products	Ref.
Z-type heterojunction	Vis light	Hydrothermal + grinding	10.94	95.63	150	Small-molecule minerals	[193]
magnetic basis	Vis light	pyrolysis	10.00	95.30	300	Magnetic recyclable	[194]
Mxene	Vis light	Ultrasound Assist	35	98.36	124	None	[195]
core–shell structure	Vis light	epitaxial growth	50	92.9	100	None	[196]
MOF-based	UV	a facile one-pot solvent–thermal precipitation	10	95	150	None	[43]
Element doping	Vis light	sol–gel	20	97.5	120	None	[197]
Mesoporous material-loaded	Vis light	sequential deposition	10	94	40	Lower-oxidation-capacity minerals	[87]
Carbon quantum dot	Full-spectrum irradiation	hydrothermal	20	100	120	None	[106]
Floatation-based photocatalysts	UV	3D printing design + surface deposition	30	93.6	240	None	[116]
Aerogel-based photocatalysts	Vis light	one-step in situ preparation	-	96.5	90	None	[177]
Molecularly imprinted photocatalysts	Vis light	surface molecular-imprinting technology	50	99	20	None	[188]
Biomimetic photocatalysts	Vis light	a novel electrochemical synthesis method	90	>99	90	Biomass ash (effective peroxymonosulphate activators for TC mineralization.	[192]

Metal–Organic Frameworks (MOFs) have demonstrated significant potential in photocatalysis, due to their high surface area, tunable porosity, and unsaturated active sites. Recent advancements, such as the integration of metal components (e.g., iron) and the development of S-type heterojunctions, have further enhanced their photocatalytic efficiency by reducing carrier recombination and improving oxidation–reduction capacities. These innovations have led to superior performance in the degradation of organic pollutants, making MOF-based photocatalysts, particularly those with S-type heterojunctions, a promising solution for environmental remediation under visible light. Future research could focus on increasing their multifunctionality, enhancing photoresponsiveness, improving catalytic efficiency, and ensuring long-term stability, with an emphasis on expanding their spectral response to enhance visible and near-infrared light absorption.

Element doping, both metal (e.g., Al, Fe, Mn) and non-metal (e.g., N, S), has been proven to improve photocatalytic performance by narrowing the bandgap, enhancing visible light absorption, and promoting charge carrier transport. Doped materials exhibit extended light-absorption spectra, optimized charge separation, and improved degradation of pollutants like tetracycline. The future direction could focus on optimizing doping types and concentrations to further enhance photocatalytic efficiency, stability, and green synthesis methods for long-term applications in environmental remediation.

Mesoporous materials (2–50 nm pore size), such as carbon-based materials, metal oxides, and MOFs, are increasingly recognized for their ability to enhance catalytic efficiency by reducing agglomeration and improving charge transfer. However, challenges such as low thermal stability remain, and future research could focus on optimizing pore structures

and enhancing material stability. Additionally, the development of carbon quantum dots (CQDs) derived from renewable sources like rice husk will focus on improving synthesis methods, thermal stability, and light absorption.

Floating photocatalysts, including both support-type and self-floating designs, offer enhanced stability and efficient light absorption. Research should also focus on integrating photocatalysis with electrophotocatalysis and optimizing real-time monitoring for enhanced pharmaceutical-wastewater treatment.

Type II and S-scheme heterojunctions, in particular, reduce recombination and expand light absorption, while Z-scheme systems separate oxidation and reduction reactions. Integrating materials like noble metals or narrow-bandgap semiconductors further boosts performance for pollutant degradation and energy conversion. Future research on heterojunction photocatalysts could focus more on the photocatalytic effects of ultraviolet and near-infrared light, expanding the spectral response range to enhance photocatalytic efficiency.

From the perspective of the catalyst itself, a strategic design optimization addressing the three critical factors influencing performance—specifically, minimizing the bandgap of the photocatalyst, mitigating surface charge recombination, enhancing carrier transfer dynamics, improving spectral absorption capacity and facilitating efficient persulfate activation—can substantially enhance photocatalytic performance. This targeted methodology is expected to significantly elevate the efficiency of photocatalytic degradation processes. From the perspective of the intrinsic characteristics of degradable target pollutants, a comprehensive structural analysis of tetracycline antibiotics—one of the representative contaminants discussed in this study—is warranted. This analysis should encompass their initial molecular structure, intermediate species formed during degradation processes, and final degradation products. Additionally, real-time monitoring of these reactions will facilitate the design of tailored photocatalyst morphologies that align with the distinct structural features observed at various reaction stages.

It is feasible to develop targeted recognition elements with high specificity through in situ growth on the surfaces of photocatalysts. This approach aims to enhance selectivity within actual aquatic environments and promote more effective degradation. Capitalizing on built-in electric fields as an intrinsic driving force for enhancing charge-carrier separation efficiency is essential. By addressing the electronegative properties inherent to antibiotic molecules and modulating surface anisotropy to alter surface electronegativity via crystal plane engineering, one can generate robust internal electric fields that hinder rapid charge recombination. This enables efficient spatial separation of electrons and holes across different facets of photocatalytic particles. In addition, within the overarching framework of green energy cycles aligned with national "dual carbon" initiatives, strategies aimed at reducing solubility rates for active components in photocatalysts while increasing their reusability are critical. Minimizing environmental toxicity associated with nanoscale photocatalytic composites constitutes an effective response to national sustainability objectives.

While current research have demonstrated the effectiveness of photocatalytic technology in the degradation of tetracycline, there is still a lack of information regarding whether the degradation products meet regulatory standards for safe discharge into the environment. Future studies should focus on quantifying the chemical properties and biological toxicity of tetracycline degradation products to assess their environmental risks and guide safe discharge practices.

Author Contributions: J.M.: methodology, formal analysis, writing—original draft, visualization. Y.C.: visualization, writing—original draft (partly). G.Z.: writing—review and editing, visualization. H.G.: writing—review and editing. H.L.: conceptualization, methodology, resources, writing—review and editing, supervision, project administration, funding acquisition. All authors have read and agreed to the published version of the manuscript.

Data Availability Statement: No new data were created or analyzed in this study. Data sharing is not applicable to this article.

Conflicts of Interest: Author Gang Zhou was employed by the company Zhejiang Province Environmental Engineering Co., Ltd. The remaining authors declare that the research was conducted in the absence of any commercial or financial relationships that could be construed as a potential conflict of interest.

References

1. Ahmaruzzaman, M.; Mishra, S.R.; Gadore, V.; Yadav, G.; Roy, S.; Bhattacharjee, B.; Bhuyan, A.; Hazarika, B.; Darabdhara, J.; Kumari, K. Phenolic Compounds in Water: From Toxicity and Source to Sustainable Solutions—An Integrated Review of Removal Methods, Advanced Technologies, Cost Analysis, and Future Prospects. *J. Environ. Chem. Eng.* **2024**, *12*, 112964. [CrossRef]
2. Zhang, K.; Wang, L.; Hong, Y.; Duan, X.; Ai, C.; Zhang, L.; Zhang, T.; Chen, Y.; Lin, X.; Shi, W.; et al. Iron Phthalocyanine Nanodots Decorated Ultra-Thin Porous Carbon Nitride: A Combination of Photocatalysis and Fenton Reaction to Achieve Two-Channel Efficient Tetracycline Degradation. *J. Alloys Compd.* **2023**, *966*, 171580. [CrossRef]
3. Jia, W.; Song, C.; He, L.; Wang, B.; Gao, F.; Zhang, M.; Ying, G. Antibiotics in Soil and Water: Occurrence, Fate, and Risk. *Curr. Opin. Environ. Sci. Health* **2023**, *32*, 100437. [CrossRef]
4. Pino-Otín, M.R.; Valenzuela, A.; Gan, C.; Lorca, G.; Ferrando, N.; Langa, E.; Ballestero, D. Ecotoxicity of Five Veterinary Antibiotics on Indicator Organisms and Water and Soil Communities. *Ecotoxicol. Environ. Saf.* **2024**, *274*, 116185. [CrossRef] [PubMed]
5. Perez-Bou, L.; Gonzalez-Martinez, A.; Gonzalez-Lopez, J.; Correa-Galeote, D. Promising Bioprocesses for the Efficient Removal of Antibiotics and Antibiotic-Resistance Genes from Urban and Hospital Wastewaters: Potentialities of Aerobic Granular Systems. *Environ. Pollut.* **2024**, *342*, 123115. [CrossRef]
6. Chang, D.; Mao, Y.; Qiu, W.; Wu, Y.; Cai, B. The Source and Distribution of Tetracycline Antibiotics in China: A Review. *Toxics* **2023**, *11*, 214. [CrossRef]
7. Martínez, J.L. Antibiotics and Antibiotic Resistance Genes in Natural Environments. *Science* **2008**, *321*, 365–367. [CrossRef]
8. World Health Organization. *Antimicrobial Resistance: Global Report on Surveillance*; World Health Organization: Geneva, Switzerland, 2014; ISBN 978-92-4-156474-8.
9. Kumar, R.; Barakat, M.A.; Al-Mur, B.A.; Alseroury, F.A.; Eniola, J.O. Photocatalytic Degradation of Cefoxitin Sodium Antibiotic Using Novel $BN/CdAl_2O_4$ Composite. *J. Clean. Prod.* **2020**, *246*, 119076. [CrossRef]
10. Zheng, X.; Wang, M.; Zhang, S.; Yangcuo, Z.; He, L.; Xie, L.; Ye, Y.; Xu, G.; Chen, Z.; Cai, Q. Development of a New Synchronous Fluorescence Spectrometry Combined with Al^{3+} Sensitized for Simultaneous and Rapid Determination of Trace Flumequine, Ciprofloxacin and Doxycycline Hydrochloride Residues in Wastewater. *Water Res.* **2024**, *260*, 121941. [CrossRef]
11. Xu, L.; Zhang, H.; Xiong, P.; Zhu, Q.; Liao, C.; Jiang, G. Occurrence, Fate, and Risk Assessment of Typical Tetracycline Antibiotics in the Aquatic Environment: A Review. *Sci. Total Environ.* **2021**, *753*, 141975. [CrossRef]
12. Yang, S.; Carlson, K. Evolution of Antibiotic Occurrence in a River through Pristine, Urban and Agricultural Landscapes. *Water Res.* **2003**, *37*, 4645–4656. [CrossRef] [PubMed]
13. Wu, D.; Dai, S.; Feng, H.; Karunaratne, S.H.P.P.; Yang, M.; Zhang, Y. Persistence and Potential Risks of Tetracyclines and Their Transformation Products in Two Typical Different Animal Manure Composting Treatments. *Environ. Pollut* **2024**, *341*, 122904. [CrossRef]
14. Zhang, G.; Zhang, C.; Liu, J.; Zhang, Y.; Fu, W. Occurrence, Fate, and Risk Assessment of Antibiotics in Conventional and Advanced Drinking Water Treatment Systems: From Source to Tap. *J. Environ. Manag.* **2024**, *358*, 120746. [CrossRef]
15. Velempini, T.; Prabakaran, E.; Pillay, K. Recent Developments in the Use of Metal Oxides for Photocatalytic Degradation of Pharmaceutical Pollutants in Water—A Review. *Mater. Today Chem.* **2021**, *19*, 100380. [CrossRef]
16. Singh, S.; Mishra, P.; Upadhyay, S. Recent Developments in Photocatalytic Degradation of Insecticides and Pesticides. *Rev. Chem. Eng.* **2021**, *39*, 225–270. [CrossRef]
17. Guo, J.; Huang, M.; Gao, P.; Zhang, Y.; Chen, H.; Zheng, S.; Mu, T.; Luo, X. Simultaneous Robust Removal of Tetracycline and Tetracycline Resistance Genes by a Novel UiO/TPU/PSF Forward Osmosis Membrane. *Chem. Eng. J.* **2020**, *398*, 125604. [CrossRef]
18. Ghuge, S.P.; Saroha, A.K. Catalytic Ozonation for the Treatment of Synthetic and Industrial Effluents—Application of Mesoporous Materials: A Review. *J. Environ. Manag.* **2018**, *211*, 83–102. [CrossRef]
19. Wang, S.; Wang, J. Activation of Peroxymonosulfate by Sludge-Derived Biochar for the Degradation of Triclosan in Water and Wastewater. *Chem. Eng. J.* **2019**, *356*, 350–358. [CrossRef]
20. Xue, Z.; Luan, D.; Zhang, H.; Lou, X.W.D. Single-Atom Catalysts for Photocatalytic Energy Conversion. *Joule* **2022**, *6*, 92–133. [CrossRef]
21. Liu, J.; Wang, G.; Li, B.; Ma, X.; Hu, Y.; Cheng, H. A High-Efficiency Mediator-Free Z-Scheme Bi_2MoO_6/AgI Heterojunction with Enhanced Photocatalytic Performance. *Sci. Total Environ.* **2021**, *784*, 147227. [CrossRef]

22. Qiu, J.; Meng, K.; Zhang, Y.; Cheng, B.; Zhang, J.; Wang, L.; Yu, J. COF/ln$_2$S$_3$ S-Scheme Photocatalyst with Enhanced Light Absorption and H$_2$O$_2$-Production Activity and fs-TA Investigation. *Adv. Mater.* **2024**, *36*, 2400288. [CrossRef] [PubMed]

23. Di, T.; Xu, Q.; Ho, W.; Tang, H.; Xiang, Q.; Yu, J. Review on Metal Sulphide-based Z-scheme Photocatalysts. *ChemCatChem* **2019**, *11*, 1394–1411. [CrossRef]

24. Liu, M.; Ye, P.; Wang, M.; Wang, L.; Wu, C.; Xu, J.; Chen, Y. 2D/2D Bi-MOF-Derived BiOCl/MoS$_2$ Nanosheets S-Scheme Heterojunction for Effective Photocatalytic Degradation. *J. Environ. Chem. Eng.* **2022**, *10*, 108436. [CrossRef]

25. Li, L.; Chao, M.; Zhang, B.; Song, C.; Luo, C.; Yan, L. A Sulfur-Doped Alga-like g-C3N4 Photocatalyst for Enhanced Photocatalytic and Antimicrobial Properties. *New J. Chem.* **2024**, *48*, 7845–7855. [CrossRef]

26. Zhang, M.; Lai, C.; Li, B.; Xu, F.; Huang, D.; Liu, S.; Qin, L.; Fu, Y.; Liu, X.; Yi, H.; et al. Unravelling the Role of Dual Quantum Dots Cocatalyst in 0D/2D Heterojunction Photocatalyst for Promoting Photocatalytic Organic Pollutant Degradation. *Chem. Eng. J.* **2020**, *396*, 125343. [CrossRef]

27. Saleem, S.; Kaur, K.; Kumar, V.; Khan, A.A.; Malik, A. An Overview of Metal–Organic Frameworks as Potential Platform: Sensing for Detection Environmental Pollutants and Drug Delivery Applications. *J. Mol. Struct.* **2024**, *1312*, 138389. [CrossRef]

28. Li, F.; Cheng, L.; Fan, J.; Xiang, Q. Steering the Behavior of Photogenerated Carriers in Semiconductor Photocatalysts: A New Insight and Perspective. *J. Mater. Chem. A* **2021**, *9*, 23765–23782. [CrossRef]

29. Wang, Z.; Yue, X.; Xiang, Q. MOFs-Based S-Scheme Heterojunction Photocatalysts. *Coord. Chem. Rev.* **2024**, *504*, 215674. [CrossRef]

30. Liu, Y.; Tang, C.; Cheng, M.; Chen, M.; Chen, S.; Lei, L.; Chen, Y.; Yi, H.; Fu, Y.; Li, L. Polyoxometalate@Metal–Organic Framework Composites as Effective Photocatalysts. *ACS Catal.* **2021**, *11*, 13374–13396. [CrossRef]

31. Cao, C.; Wang, J.; Yu, X.; Zhang, Y.; Zhu, L. Photodegradation of Seven Bisphenol Analogues by Bi$_5$O$_7$I/UiO-67 Heterojunction: Relationship between the Chemical Structures and Removal Efficiency. *Appl. Catal. B Environ.* **2020**, *277*, 119222. [CrossRef]

32. Zhang, L.; Wang, C.; Wang, C. Mining Resources from Wastes to Produce High Value-Added MOFs. *Resour. Conserv. Recycl.* **2023**, *190*, 106805. [CrossRef]

33. Wang, F.; Gao, Y.; Liu, S.; Yi, X.; Wang, C.; Fu, H. Fabrication Strategies of Metal–Organic Frameworks Derivatives for Catalytic Aqueous Pollutants Elimination. *Chem. Eng. J.* **2023**, *463*, 142466. [CrossRef]

34. Zhang, R.; Jia, K.; Xue, Z.; Hu, Z.; Yuan, N. Modulation of CdS Nanoparticles Decorated Bimetallic Fe/Mn-MOFs Z-Scheme Heterojunctions for Enhancing Photocatalytic Degradation of Tetracycline. *J. Alloys Compd.* **2024**, *992*, 174462. [CrossRef]

35. Xu, M.; Zhang, R.; He, J.; Li, Z.; Liu, Y.; Chen, D.; Peng, L.; Shu, Y.; Jiang, L.; Zhao, G. Construction of g-C$_3$N$_4$@Bi-MOF@BiOCl Double Z-Type Heterojunctions for Photodegradation of Antibiotics under Visible Light Irradiation: Mechanism, Pathway, and Toxicity Assessment. *J. Water Process Eng.* **2024**, *66*, 106036. [CrossRef]

36. Wang, Y.; Xue, S.; Liao, Y.; Lu, Q.; Wang, H.; Zhao, C.; Tang, N.; Du, F. MOF-Derived Bi$_{12}$O$_{17}$Cl$_2$ Nanoflakes for the Photocatalytic Degradation of Bisphenol A and Tetracycline Hydrochloride under Visible Light. *ACS Appl. Nano Mater.* **2024**, *7*, 3188–3198. [CrossRef]

37. Chen, H.; Cai, T.; Dong, W.; Wang, J.; Liu, Y.; Li, W.; Xia, X.; Tang, L. Catalytic Thermal Degradation of Tetracycline Based on Iron-Based MOFs and Annealed Derivative in Dark Condition. *J. Clean. Prod.* **2023**, *406*, 136976. [CrossRef]

38. Gagliardi, L.; Yaghi, O.M. Three Future Directions for Metal–Organic Frameworks. *Chem. Mater.* **2023**, *35*, 5711–5712. [CrossRef]

39. Tai, R.; Wu, R.; Zhang, M.; Yuan, J.; Tressel, J.; Tang, Y.; Wang, Q.; Chen, S. Metal–Organic Framework–Based Heterojunctions for Photocatalysis. *Curr. Opin. Chem. Eng.* **2024**, *45*, 101033. [CrossRef]

40. Li, F.; Zhu, G.; Jiang, J.; Yang, L.; Deng, F.; Arramel; Li, X. A Review of Updated S-Scheme Heterojunction Photocatalysts. *J. Mater. Sci. Technol.* **2024**, *177*, 142–180. [CrossRef]

41. Luo, C.; Lin, Y.; Zhang, Y.; Zhang, S.; Tong, S.; Wu, S.; Yang, C. S-Scheme Heterojunction between MOFs and Ag$_3$PO$_4$ Leads to Efficient Photodegradation of Antibiotics in Swine Wastewater. *Sep. Purif. Technol.* **2023**, *320*, 124052. [CrossRef]

42. Zhang, S.; Han, D.; Wang, Z.; Gu, F. Bi-Doped and Bi Nanoparticles Loaded CeO$_2$ Derived from Ce-MOF for Photocatalytic Degradation of Formaldehyde Gas and Tetracycline Hydrochloride. *Small* **2024**, *20*, 2309656. [CrossRef] [PubMed]

43. Sheikhsamany, R.; Nezamzadeh-Ejhieh, A.; Ensandoost, R.; Kakavandi, B. BaTi$_{0.85}$Zr$_{0.15}$O$_3$/MOF-5 Nanocomposite: Synthesis, Characterization and Photocatalytic Activity toward Tetracycline. *J. Mol. Liq.* **2024**, *403*, 124850. [CrossRef]

44. Roy, D.; Sarkar, P.; Chowdhury, A.; Zade, S.U.; De, S. Preparation and Performance of Scalable Photocatalyst Beads: A Case Study of Tetracycline Degradation Assisted by Visible Light and Peroxymonosulfate Activation. *J. Clean. Prod.* **2024**, *447*, 141548. [CrossRef]

45. Manju, R.; Jeyaprakash, J.S.; Yazhini, C.; Neppolian, B. Wide-Spectrum-Responsive MoS$_2$/WS$_2$ Decorated Al-MOF Nanohybrid with Dual S-Scheme Heterojunction in Facilitating Sonophotocatalytic Tetracycline Abatement and Pharmaceutical Effluent Treatment. *J. Clean. Prod.* **2024**, *476*, 143752. [CrossRef]

46. Zhao, R.; Hu, F.; Zhang, Y.; Dong, B.; Li, Z.; Qu, W.; Liu, C.; Song, Z.; Lu, P.; Ji, D.; et al. Carbon Quantum Dots/UiO-66@polysulfone Porous Microspheres Fabricated via Pickering Emulsion Template for Pollutant Removal. *Sep. Purif. Technol.* **2024**, *337*, 126367. [CrossRef]

47. Xu, M.; Zhang, R.; He, J.; Chen, Z.; Jiang, J.; Li, Z.; Liu, Y.; Chen, D.; Ma, Y. Construction of Heterojunctions with in Situ Growth of ZnIn$_2$S$_4$ Nanosheets on the Surface of Atomically Dispersed Cu-Modified MOFs for High-Performance Visible-Light Photocatalytic Antibiotic Degradation. *Sep. Purif. Technol.* **2025**, *354*, 129093. [CrossRef]

48. Wen, Q.; Li, D.; Gao, C.; Wu, L.; Song, F.; Zhou, J. Synthesis of Dual p–n Heterojunction of Ni/Mn-MOF-74/CdS@Co$_3$O$_4$ Photocatalyst as a Photoassisted Fenton-like Catalyst for Removal of Tetracycline Hydrochloride. *Inorg. Chem.* **2023**, *62*, 20412–20429. [CrossRef]

49. Sun, X.; Fang, Y.; Mu, J.; Zhao, W.; Wang, J.; Liu, B.; Cao, Y. One-Step Synthesis of Mixed-Valence NH$_2$-MIL-101(Fe^{2+}/Fe^{3+}) with Controllable Morphology for Photocatalytic Removal of Tetracycline and Cr(VI). *J. Alloys Compd.* **2023**, *955*, 169969. [CrossRef]

50. Hu, H.; Lin, H.; Chen, X.; Pan, Y.; Li, X.; Zhuang, Z.; Chen, H.; Wang, X.; Luo, M.; Zheng, K.; et al. Fe, Mn-Prussian Blue analogue@MXene Composites for Efficient Photocatalytic Peroxydisulfate-Activated Degradation of Tetracycline Hydrochloride and Photoelectrochemical Desalination. *Chem. Eng. J.* **2023**, *476*, 146682. [CrossRef]

51. Jin, W.; Yang, C.; Pau, R.; Wang, Q.; Tekelenburg, E.K.; Wu, H.; Wu, Z.; Jeong, S.Y.; Pitzalis, F.; Liu, T.; et al. Photocatalytic Doping of Organic Semiconductors. *Nature* **2024**, *630*, 96–101. [CrossRef]

52. Sun, Y.; Zhao, L.; Yang, J.; Wang, X.; Peng, H.; Peng, J. Evaporation-Induced Self-Assembly Al Doped Black TiO$_2$ for the Degradation of Tetracycline Hydrochloride under Visible Light. *J. Alloys Compd.* **2024**, *1007*, 176415. [CrossRef]

53. Dai, H.; Liu, Z.; Ou, L.; Shen, Y.; Ning, Z.; Hu, F.; Peng, X. Iron Nanoparticles Decorated TiO$_2$ Hollow Microspheres for Boosting Degradation of Tetracycline in a Photo-Fenton Catalytic System. *J. Environ. Chem. Eng.* **2023**, *11*, 110797. [CrossRef]

54. Xie, Q.; Huang, H.; Zhang, C.; Shi, H. Regulating Spin Polarization of Mn-Doped ZnFe$_2$O$_4$ for Boosting Antibiotic Degradation: Intermediate, Toxicity Assessment and Mechanism. *J. Clean. Prod.* **2024**, *466*, 142886. [CrossRef]

55. Chen, M.; Cai, X.; Yang, Q.; Lu, W.; Huang, Z.; Gan, T.; Hu, H.; Zhang, Y. Construction of a N–Mo–O Bond Bridged MoO$_2$/Mo-Doped g-C$_3$N$_4$ Schottky Heterojunction Composite with Enhanced Interfacial Compatibility for Efficient Photocatalytic Degradation of Tetracycline. *Sep. Purif. Technol.* **2023**, *314*, 123546. [CrossRef]

56. Wang, F.; Zhang, W.; Liu, H.; Cao, R.; Meng, C. Roles of CeO$_2$ in preparing Ce-doped CdIn$_2$S$_4$ with boosted photocatalytic degradation performance for methyl orange and tetracycline hydrochloride. *Chemosphere* **2023**, *338*, 139574. [CrossRef] [PubMed]

57. Zhang, H.; Luo, W.; Sun, H.; Yang, H.; Yang, T.; Liu, D.; Zhu, X.; Zhao, L.; Shu, M.; Yang, F. Ce-Doped Nanosheet as Visible Light Photocatalyst for the Photocatalytic Degradation of Tetracycline Hydrochloride. *ACS Appl. Nano Mater.* **2024**, *7*, 11506–11517. [CrossRef]

58. Bilgin Simsek, E.; Tuna, Ö. Understanding the Nature of Ce–Fe Synergy in the Structure CaWO$_4$ Scheelite for Enhanced Photocatalytic Performance under Visible Light. *Ceram. Int.* **2024**, *50*, 20600–20611. [CrossRef]

59. Zhou, M.; Huang, X.; Zhang, Y.; Zhou, N.; Deng, J.; Zeng, Y.; Lin, D.; Zhou, C.; Liu, Q. Synergistic Combination of Mn/Fe Bimetal-Doped Carbon Nitride and Peroxymonosulfate for Efficient Photocatalytic Degradation of Antibiotics. *J. Environ. Chem. Eng.* **2024**, *12*, 113730. [CrossRef]

60. Wang, H.; Wan, Y.; Li, B.; Ye, J.; Gan, J.; Liu, J.; Liu, X.; Song, X.; Zhou, W.; Li, X.; et al. Rational Design of Ce-Doped CdS/N-rGO Photocatalyst Enhanced Interfacial Charges Transfer for High Effective Degradation of Tetracycline. *J. Mater. Sci. Technol.* **2024**, *173*, 137–148. [CrossRef]

61. Li, Y.; Qu, C.; Ye, Q.; Meng, F.; Yang, D.; Wang, L. Enhanced Tetracycline Degradation by Novel Mn–FeOOH/CNNS Photocatalysts in a Visible-Light-Driven Photocatalysis Coupled Peroxydisulfate System. *Environ. Res.* **2024**, *257*, 119293. [CrossRef]

62. Xing, Y.; Jiang, X.; Han, L.; Jin, X.; Ni, G.; Peng, Y.; Yong, X.; Wang, X. Efficient Degradation of Tetracycline over Vacancy-Modified Cu-Doped Bi$_2$O$_2$S via Peroxymonosulfate Activation and Photocatalysis. *J. Clean. Prod.* **2023**, *400*, 136631. [CrossRef]

63. Chen, H.; Meng, F.; Feng, X.; Zhao, Y.; Xie, T.; Wang, D.; Lin, Y. Efficient Photocatalytic Activation of Peroxymonosulfate by Cobalt-Doped Oxygen-Vacancies-Rich BiVO$_4$ for Rapid Tetracycline Degradation. *Langmuir* **2024**, *40*, 12778–12791. [CrossRef]

64. Li, S.; Deng, C.; Karmaker, P.G.; Yang, K.; Wang, J.; Liu, W.; Yang, X. Yb-Doped BiOBr for Highly Efficient Photocatalytic Degradation of Tetracycline Hydrochloride under Visible Light Irradiation. *Mater. Res. Bull.* **2024**, *178*, 112895. [CrossRef]

65. Luo, X.; Zhu, P.; Zeng, J.; Liang, T.; Qiu, Q. Enhanced Photocatalytic Degradation by the Preparation of a Stable La-Doped FeTiO$_3$ Photocatalyst: Experimental and DFT Study. *Inorg. Chem.* **2024**, *63*, 14425–14437. [CrossRef]

66. James, A.; Shivakumar; Rodney, J.D.; Joshi, S.; Dalimba, U.; Kim, B.C.; Udayashankar, N.K. Mechanistic Insights and DFT Analysis of Bimetal Doped Styrofoam-like LaFeO$_3$ Perovskites with in-Built Dual Redox Couples for Enhanced Photo-Fenton Degradation of Tetracycline. *Chem. Eng. J.* **2024**, *481*, 148466. [CrossRef]

67. Zhang, S.; Li, J.; Wang, X.; Huang, Y.; Zeng, M.; Xu, J. In Situ Ion Exchange Synthesis of Strongly Coupled Ag@AgCl/g-C$_3$N$_4$ Porous Nanosheets as Plasmonic Photocatalyst for Highly Efficient Visible-Light Photocatalysis. *ACS Appl. Mater. Interfaces* **2014**, *6*, 22116–22125. [CrossRef]

68. Qu, J.; Du, Y.; Feng, Y.; Wang, J.; He, B.; Du, M.; Liu, Y.; Jiang, N. Visible-Light-Responsive K-Doped g-C$_3$N$_4$/BiOBr Hybrid Photocatalyst with Highly Efficient Degradation of Rhodamine B and Tetracycline. *Mater. Sci. Semicond. Process.* **2020**, *112*, 105023. [CrossRef]

69. Wang, W.; Zeng, Z.; Zeng, G.; Zhang, C.; Xiao, R.; Zhou, C.; Xiong, W.; Yang, Y.; Lei, L.; Liu, Y.; et al. Sulfur Doped Carbon Quantum Dots Loaded Hollow Tubular G-C$_3$N$_4$ as Novel Photocatalyst for Destruction of Escherichia Coli and Tetracycline Degradation under Visible Light. *Chem. Eng. J.* **2019**, *378*, 122132. [CrossRef]

70. Jia, H.; Dong, M.; Yuan, Z.; Chen, J.; Gong, Z.; Shao, J. Deep Eutectic Solvent Electrolysis for Preparing N and P Co-Doped Titanium Dioxide for Rapid Photodegradation of Dyestuff and Antibiotic. *Ceram. Int.* **2021**, *47*, 23249–23258. [CrossRef]

71. Tao, F.-T.; Hu, C.; Wu, J.C.S.; Nguyen, V.-H.; Tung, K.-L. Influence of Nitrogen Sources on N-Doped Reduced TiO$_2$ Prepared Using Atmospheric Plasma Spraying for Photocatalytic Tetracycline and Ciprofloxacin Degradation. *Sep. Purif. Technol.* **2023**, *326*, 124784. [CrossRef]

72. Zhao, E.; Li, M.; Xu, B.; Wang, X.; Jing, Y.; Ma, D.; Mitchell, S.; Pérez-Ramírez, J.; Chen, Z. Transfer Hydrogenation with a Carbon-Nitride-Supported Palladium Single-Atom Photocatalyst and Water as a Proton Source. *Angew. Chem. Int. Ed.* **2022**, *61*, e202207410. [CrossRef]

73. Ali, A.; Shoeb, M.; Li, Y.; Li, B.; Khan, M.A. Enhanced Photocatalytic Degradation of Antibiotic Drug and Dye Pollutants by Graphene-Ordered Mesoporous Silica (SBA 15)/TiO$_2$ Nanocomposite under Visible-Light Irradiation. *J. Mol. Liq.* **2021**, *324*, 114696. [CrossRef]

74. Wang, P.; Zhang, X.; Shi, R.; Zhao, J.; Waterhouse, G.I.N.; Tang, J.; Zhang, T. Photocatalytic Ethylene Production by Oxidative Dehydrogenation of Ethane with Dioxygen on ZnO-Supported PdZn Intermetallic Nanoparticles. *Nat. Commun.* **2024**, *15*, 789. [CrossRef]

75. Wu, C.; Shen, Q.; Zheng, S.; Zhang, X.; Sheng, J.; Yang, H. Fabrication of Bi$_2$Sn$_2$O$_7$@MIL-100(Fe) Composite Photocatalyst with Enhanced Superoxide-Radical-Dominated Photocatalytic Activity for Ciprofloxacin Degradation. *J. Mol. Struct.* **2022**, *1258*, 132657. [CrossRef]

76. Razavi-Esfali, M.; Mahvelati-Shamsabadi, T.; Fattahimoghaddam, H.; Lee, B.-K. Highly Efficient Photocatalytic Degradation of Organic Pollutants by Mesoporous Graphitic Carbon Nitride Bonded with Cyano Groups. *Chem. Eng. J.* **2021**, *419*, 129503. [CrossRef]

77. Tang, H.; E, H.; Yao, C.; Wang, X.; Zhou, J.; Song, W.; Zhang, Z. Boosted Antibiotic Elimination over 2D/2D Mesoporous CeO$_2$/BiOCl S-Scheme Photocatalyst. *Sep. Purif. Technol.* **2025**, *354*, 128977. [CrossRef]

78. Kılıç, D.; Sevim, M.; Eroğlu, Z.; Metin, Ö.; Karaca, S. Strontium Oxide Modified Mesoporous Graphitic Carbon Nitride/Titanium Dioxide Nanocomposites (SrO-Mpg-CN/TiO$_2$) as Efficient Heterojunction Photocatalysts for the Degradation of Tetracycline in Water. *Adv. Powder Technol.* **2021**, *32*, 2743–2757. [CrossRef]

79. Li, J.; Li, R.; Wang, W.; Lan, K.; Zhao, D. Ordered Mesoporous Crystalline Frameworks Toward Promising Energy Applications. *Adv. Mater.* **2024**, *36*, 2311460. [CrossRef]

80. Wei, Y.; Chen, M.; Guo, S.; Li, Y.; Zhang, Z.; Xie, Y.; Cai, C.; Wei, Q. Hierarchically Porous TiO$_2$ Photocatalyst Prepared by Additive Manufacturing and Dealloying for Highly Efficient Photocatalytic Degradation of Tetracycline. *ACS ES&T Water* **2024**, *4*, 1590–1600. [CrossRef]

81. Phoon, B.; Lai, C.; Chen, C.; Boonyuen, S.; Tang, W.; Juan, J. Mesoporous I-Doped-g-C$_3$N$_4$ with C Vacancies as Superior Visible-Light-Driven Photocatalyst for Removal of Tetracycline Antibiotic. *J. Alloys Compd.* **2024**, *1009*, 176772. [CrossRef]

82. Jiang, Y.; Wang, Z.; Zhou, Q.; Yang, P.; Qin, P.; Huang, F.; Yang, W. Highly Effective Ruthenium-Doped Mesoporous Ti$_{1-x}$Ru$_x$O$_{2-y}$ Crystals for Photocatalytic Tetracycline Degradation. *J. Mater. Chem. C* **2023**, *11*, 11027–11033. [CrossRef]

83. Shanmugam, P.; Smith, S.M.; Boonyuen, S.; Luengnaruemitchai, A. In-Situ Development of Boron Doped g-C$_3$N$_4$ Supported SBA-15 Nanocomposites for Photocatalytic Degradation of Tetracycline. *Environ. Res.* **2023**, *224*, 115496. [CrossRef]

84. Mkhalid, I.A.; Ismail, A.A.; Hussein, M.A.; Thomali, R.H.M.A. Nanoheterojunctions MnCo$_2$O$_4$ Nanoparticles Anchored on Mesoporous TiO$_2$ Networks for Superior Photocatalytic Ability. *Mater. Res. Bull.* **2023**, *167*, 112439. [CrossRef]

85. Tang, Q.; Cheng, Q.; Pan, Z. Constructing Novel Metal-Free HCOF-Ph@g-C$_3$N$_4$ Heterojunctions through Molecular Expansion to Enhance Photogenerated Carrier Involved Molecular Oxygen Activation and Photocatalytic Hydrogen Evolution. *Sustain. Mater. Technol.* **2024**, *41*, e01115. [CrossRef]

86. Das, C.; Shafi, T.; Thulluru, L.P.; Li, Y.; Naushad, M.; Dubey, B.K.; Chowdhury, S. Three-Dimensional Highly Porous MoS$_2$/Graphene Aerogel for Visible-Light-Driven Photocatalytic Degradation of Tetracycline. *ACS ES&T Water* **2024**, *4*, 2144–2158. [CrossRef]

87. Hou, Y.; Meng, F.; He, J.; Dong, M.; Tong, J.; Sun, J.; Sun, C.; Wang, X.; Su, Z. Hierarchically Porous CsPbBr$_3$@HZIF-8 Heterojunctions for High-Performance Photocatalytic Degradation of Antibiotics in High-Salinity Wastewater. *J. Mater. Chem.* **2023**, *11*, 13570–13578. [CrossRef]

88. Zhu, L.; Ge, X.; Yu, H.; Li, C.; Wang, Q.; Zhang, W.; Wang, X.; Liu, X. Preparation of O-g-C$_3$N$_4$ Nanowires/Bi$_2$O$_2$CO$_3$ Porous Plate Composite Photocatalysts for the Efficient Degradation of Tetracycline Hydrochloride in Wastewater. *Environ. Res.* **2024**, *251*, 118566. [CrossRef]

89. Khan, M.A.; Safira, A.R.; Kaseem, M.; Fattah-alhosseini, A. Enhanced Electrochemical and Photocatalytic Performance Achieved through Dual Incorporation of SnO$_2$ and WO$_3$ Nanoparticles into LDH Layer Fabricated on PEO-Coated AZ31 Mg Alloy. *J. Magnes. Alloys* **2024**, *12*, 1880–1898. [CrossRef]

90. Guo, H.; Lu, Y.; Lei, Z.; Bao, H.; Zhang, M.; Wang, Z.; Guan, C.; Tang, B.; Liu, Z.; Wang, L. Machine Learning-Guided Realization of Full-Color High-Quantum-Yield Carbon Quantum Dots. *Nat. Commun.* **2024**, *15*, 4843. [CrossRef]

91. Zhang, J.; Shao, C.; Zhang, A.; Zhang, Y.; Zhang, L.; Bai, H. Nitrogen-Doped Carbon Quantum Dots Modified Dual-Vacancy Z-Scheme CuFe$_2$O$_4$/g-C$_3$N$_4$ Photocatalyst Synergistic with Fenton Technique for Photothermal Degradation of Antibiotics. *Chem. Eng. J.* **2024**, *497*, 154497. [CrossRef]

92. Kumar, G.; Cilamkoti, V.; Dutta, R.K. Sunlight Mediated Enhanced Photocatalytic Degradation of Antibiotics in Aqueous Medium Using Silicon Doped Carbon Quantum Dots Decorated Bi$_2$MoO$_6$ Nanoflakes. *Colloids Surf. A Physicochem. Eng. Asp.* **2022**, *639*, 128368. [CrossRef]

93. Wang, C.; Rong, K.; Liu, Y.; Yang, F.; Li, S. Carbon Quantum Dots-Modified Tetra (4-Carboxyphenyl) Porphyrin/BiOBr S-Scheme Heterojunction for Efficient Photocatalytic Antibiotic Degradation. *Sci. China Mater.* **2024**, *67*, 562–572. [CrossRef]

94. Hu, J.; Chen, C.; Tan, C.; Fan, H.; Lu, J.; Li, Y.; Hu, H. Novel In-Situ Composites of Chlorine-Doped CQDs and g-C₃N₄ with Improved Interfacial Connectivity and Accelerated Charge Transfer to Enhance Photocatalytic Degradation of Tetracycline and Hydrogen Evolution. *Appl. Surf. Sci.* **2023**, *638*, 158060. [CrossRef]

95. Choi, N.; Tang, C.; Park, Y.; Du, A.; Ayoko, G.A.; Hwang, Y.; Chae, S. Visible-Light-Driven Photocatalytic Degradation of Tetracycline Using Citric Acid and Lemon Juice-Derived Carbon Quantum Dots Incorporated TiO₂ Nanocomposites. *Sep. Purif. Technol.* **2024**, *350*, 127836. [CrossRef]

96. Kaur, A.; Kaur, M.; Vyas, P. Abatement of Microbes and Organic Pollutants Using Heterostructural Nanocomposites of Rice Straw CQDs with Substituted Strontium Ferrite. *Chemosphere* **2024**, *359*, 142310. [CrossRef]

97. Wang, J.; Li, S.; Ma, P.; Guo, Z.; Ma, Q.; Zhao, Q.; Guo, Y.; Zhao, J.; Guan, G. Carbon Quantum Dots/Cu₂O S-Scheme Heterojunction for Enhanced Photocatalytic Degradation of Tetracycline. *Colloid Surf. A* **2024**, *690*, 133779. [CrossRef]

98. Nguyen, M.B.; Doan, H.V.; Le Hoang Tan, D.; Lam, T.D. Advanced G-C₃N₄ and Bimetallic FeNi-BTC Integration with Carbon Quantum Dots for Removal of Microplastics and Antibiotics in Aqueous Environments. *J. Environ. Chem. Eng.* **2024**, *12*, 112965. [CrossRef]

99. Nguyen, M.B.; Doan, H.V.; Tan, D.L.H.; Lam, T.D. Enhancement of Tetracycline Photocatalytic Degradation under Visible Light: Unleashing the Synergy of Z-Scheme Ag₃PO₄/GCN/FeNi-BTC Photocatalyst with Carbon Quantum Dots. *J. Ind. Eng. Chem.* 2024. *in press*. [CrossRef]

100. Chen, J.; Qin, S.; Yang, X.; Wang, Y.; Yang, T.; Que, M.; Ma, Y.; Li, Y. Synthesis of Highly Conductive Carbon Quantum Dot-Enhanced Z-Scheme BiOBr/g-C₃N₄ Heterojunction for Effective Photocatalytic Degradation of Tetracycline Hydrochloride. *J. Phys. Chem. Solids* **2024**, *189*, 111957. [CrossRef]

101. Chen, J.; Zhang, Y.; Wang, Y.; Luo, S.; Ma, C.; Zhang, H.; Guo, M. Internal Electric Field Promoted NCDs/BiOBr/AgBr Z-Scheme Heterojunction with Rich Oxygen Vacancies for Efficient Photocatalytic Degradation of Tetracycline and Reduction of Cr (VI). *J. Environ. Chem. Eng.* **2024**, *12*, 112476. [CrossRef]

102. Ma, H.; He, J.; Li, Z.; Dong, L.; Guo, S.; Zhu, X.; Li, D.; Zang, L.; Shi, L.; Ba, T. Lignin-Derived Carbon Quantum Dots/Ni-MOL Heterojunction from Red Phosphorus-Assisted Ball Milling Pretreatment and Their Application in Photocatalysis: An Insight from Experiment and DFT Calculation. *Ind. Crops Prod.* **2022**, *189*, 115829. [CrossRef]

103. Lv, M.; Wang, S.; Shi, H. Carbon Quantum Dots/BiVO₄ S-Scheme Piezo-Photocatalysts Improved Carrier Separation for Efficient Antibiotic Removal. *J. Mater. Sci. Technol.* **2024**, *201*, 21–31. [CrossRef]

104. Karaca, M.; Eroğlu, Z.; Açışlı, Ö.; Metin, Ö.; Karaca, S. Boosting Tetracycline Degradation with an S-Scheme Heterojunction of N-Doped Carbon Quantum Dots-Decorated TiO₂. *ACS Omega* **2023**, *8*, 26597–26609. [CrossRef] [PubMed]

105. Ying, W.; Liu, Q.; Jin, X.; Ding, G.; Liu, M.; Wang, P.; Chen, S. Magnetic Carbon Quantum Dots/Iron Oxide Composite Based on Waste Rice Noodle and Iron Oxide Scale: Preparation and Photocatalytic Capability. *Nanomaterials* **2023**, *13*, 2506. [CrossRef]

106. Lu, T.; Huang, H.; Lv, G.; Meng, Z.; Zhu, L. Aerogel-Derived Carbon Quantum Dots Modified BiOCl Nanocomposites with Augmented Oxygen Vacancies for Enhanced Photodegradation of Antibiotics. *J. Ind. Eng. Chem.* **2024**, *138*, 586–600. [CrossRef]

107. Chen, H.; Niu, Y.; Xu, H.; Zhang, S.; Huang, C.; Cui, Z. Construction and Investigation of Graphitic Carbon Nitride/Expanded Perlite Composite Photocatalyst with Floating Ability. *Colloid Surf. A* **2022**, *648*, 129384. [CrossRef]

108. Liu, G.; Yi, X.; Chu, H.; Wang, C.; Gao, Y.; Wang, F.; Wang, F.; Wang, P.; Wang, J. Floating MIL-88A(Fe)@expanded Perlites Catalyst for Continuous Photo-Fenton Degradation toward Tetracyclines under Artificial Light and Real Solar Light. *J. Hazard. Mater.* **2024**, *472*, 134420. [CrossRef]

109. Wang, M.; Zhang, Y.; Dong, S.; Li, N.; Xu, Q.; Li, H.; Lu, J.; Chen, D. Self-Floating Polymer Microreactor for High-Efficiency Synergistic CO2 Photoreduction and Antibiotic Degradation in One Photoredox Cycle. *Adv. Funct. Mater.* **2024**, 2408831. [CrossRef]

110. Zhang, T.; Qu, J.; Wu, J.; Jiao, F.; Li, C.; Gao, F.; Liu, J.; Yu, Z.; Li, X. All-In-One Self-Floating Wood-Based Solar-Thermal Evaporators for Simultaneous Solar Steam Generation and Catalytic Degradation. *Adv. Funct. Mater.* **2024**, *34*, 2403505. [CrossRef]

111. Swathi, A.C.; Sandhiya, S.T.; B, S.; Chandran, M. Precursor Dependent—Visible Light-Driven g-C₃N₄ Coated Polyurethane Foam for Photocatalytic Applications. *Chemosphere* **2024**, *350*, 141013. [CrossRef]

112. Lin, L.; Xie, D.; Xu, L.; Huang, Y.; Qing, X.; Huang, M.; Kazemian, H. One-Step Synthesis of Floatable BiOCl/BiOBr@FACs Enriched in Oxygen Vacancies for Improved Photocatalytic Activity via Peroxymonosulfate Activation. *Colloid Surf. A* **2023**, *676*, 132165. [CrossRef]

113. Wu, T.; Liang, Q.; Tang, L.; Tang, J.; Wang, J.; Shao, B.; Gong, S.; He, Q.; Pan, Y.; Liu, Z. Construction of a Novel S-Scheme Heterojunction Piezoelectric Photocatalyst V-BiOIO3/FTCN and Immobilization with Floatability for Tetracycline Degradation. *J. Hazard. Mater.* **2023**, *443*, 130251. [CrossRef] [PubMed]

114. Liu, Y.; Wang, X.; Sun, Q.; Chen, L.; Yuan, M.; Sun, Z.; Zhang, Y.; Xia, S.; Zhao, J. Enhanced Activation of Peroxymonosulfate by a Floating Cu0-MoS₂/C₃N₄ Photocatalyst under Visible-Light Assistance for Tetracyclines Degradation and Escherichia Coli Inactivation. *Chem. Eng. J.* **2023**, *457*, 141220. [CrossRef]

115. Zhang, M.; Ke, J.; Xu, D.; Zhang, X.; Liu, H.; Wang, Y.; Yu, J. Construction of Plasmonic Bi/Bismuth Oxycarbonate/Zinc Bismuth Oxide Ternary Heterojunction for Enhanced Charge Carrier Separation and Photocatalytic Performances. *J. Colloid Interface Sci.* **2022**, *615*, 663–673. [CrossRef]

116. Zhao, Z.-A.; Mao, J.; Lu, C.; Yang, S.; Qian, Q.; Chen, Q.; Xue, H.; Sun, X.; Yang, M.-Q. Design and Fabrication of Self-Suspending Aluminum-Plastic/Semiconductor Photocatalyst Devices for Solar Energy Conversion. *J. Environ. Sci.* **2024**, *136*, 615–625. [CrossRef] [PubMed]

117. Liu, Y.; Wang, X.; Sun, Q.; Yuan, M.; Sun, Z.; Xia, S.; Zhao, J. Enhanced Visible Light Photo-Fenton-like Degradation of Tetracyclines by Expanded Perlite Supported FeMo$_3$Ox/g-C$_3$N$_4$ Floating Z-Scheme Catalyst. *J. Hazard. Mater.* **2022**, *424*, 127387. [CrossRef] [PubMed]

118. Liu, S.; Guo, H.; Xu, Z.; Li, Z.; Qi, X. Self-Floating FeOOH/EPE Catalyst Derived from Waste Expandable Polyethylene for Boosted Peroxymonosulfate Activation for Removal of Tetracycline Hydrochloride. *J. Mater. Sci. Mater. Electron.* **2024**, *35*, 1747. [CrossRef]

119. Zhang, W.; Tan, Q.; Liu, T.; He, Y.; Chen, G.; Chen, K.; Han, D.; Qin, D.; Niu, L. Fabrication of water-floating litchi-like polystyrene-sphere-supported TiO$_2$/Bi$_2$O$_3$ S-scheme heterojunction for efficient photocatalytic degradation of tetracycline. *Mater. Horiz.* **2023**, *10*, 5869–5880. [CrossRef] [PubMed]

120. Liu, Y.; Wang, X.; Sun, Q.; Yuan, M.; Sun, Z.; Chen, L.; Zhang, Y.; Xia, S.; Zhao, J. Enhanced Activation of Peroxymonosulfate by a Floating FeMo$_3$Ox/C$_3$N$_4$ Photocatalyst under Visible-Light Assistance for Oxytetracycline Degradation: Performance, Mechanisms and Comparison with H$_2$O$_2$ Activation. *Environ. Pollut.* **2023**, *316*, 120668. [CrossRef]

121. Bai, S.; Jiang, J.; Zhang, Q.; Xiong, Y. Steering Charge Kinetics in Photocatalysis: Intersection of Materials Syntheses, Characterization Techniques and Theoretical Simulations. *Chem. Soc. Rev.* **2015**, *44*, 2893–2939. [CrossRef]

122. Xie, L.; Du, T.; Wang, J.; Ma, Y.; Ni, Y.; Liu, Z.; Zhang, L.; Yang, C.; Wang, J. Recent Advances on Heterojunction-Based Photocatalysts for the Degradation of Persistent Organic Pollutants. *Chem. Eng. J.* **2021**, *426*, 130617. [CrossRef]

123. Shang, Y.; Li, W.; Ma, Y.; Li, B.; Xu, Q.; Du, Y.; Peng, Y.; Wang, Y.; Zhu, Y. Rapid Hole Generation via D-A Structure-Dependent Built-In Electric Field of Deacetylated Chitin-PDI for Efficient Photocatalytic Oxidation. *Adv. Funct. Mater.* **2024**, 2406533. [CrossRef]

124. Zhou, H.; Qu, Y.; Zeid, T.; Duan, X. Towards Highly Efficient Photocatalysts Using Semiconductor Nanoarchitectures. *Energy Environ. Sci.* **2012**, *5*, 6732–6743. [CrossRef]

125. Acharya, L.; Nayak, S.; Pattnaik, S.P.; Acharya, R.; Parida, K. Resurrection of Boron Nitride in P-n Type-II Boron Nitride/B-Doped-g-C$_3$N$_4$ Nanocomposite during Solid-State Z-Scheme Charge Transfer Path for the Degradation of Tetracycline Hydrochloride. *J. Colloid Interface Sci.* **2020**, *566*, 211–223. [CrossRef] [PubMed]

126. Wang, Z.; Wang, S.; Xu, X.; Shi, H.; Cui, S.; Liu, W.; Tang, T. Enhanced Photocatalytic Performance of NiFe$_2$O$_4$/ZnIn$_2$S$_4$ p-n Heterojunction for Efficient Degradation of Tetracycline. *J. Colloid Interface Sci.* **2025**, *677*, 11–24. [CrossRef]

127. Yu, X.; Li, Z.; Liu, Z.; Wang, K. Fabrication of p–n Cu$_2$O/CaWO$_4$ Heterojunctions for the Efficient Degradation of Tetracycline and Doxycycline. *Appl. Surf. Sci.* **2024**, *665*, 160285. [CrossRef]

128. Li, S.; Xue, B.; Wang, C.; Jiang, W.; Hu, S.; Liu, Y.; Wang, H.; Liu, J. Facile Fabrication of Flower-Like BiOI/BiOCOOH p-n Heterojunctions for Highly Efficient Visible-Light-Driven Photocatalytic Removal of Harmful Antibiotics. *Nanomaterials* **2019**, *9*, 1571. [CrossRef] [PubMed]

129. Ma, M.; Yan, X.; Mao, Y.; Kang, H.; Yan, Q.; Zhou, J.; Song, Z.; Zhu, H.; Li, Y.; Cui, L. All-Solid-State Z-Scheme AgBr/Bi$_2$CrO$_6$ Heterostructure with Metallic Ag as a Charge Transfer Bridge for Boosted Charge Transfer and Photocatalytic Performances. *Appl. Surf. Sci.* **2024**, *654*, 159471. [CrossRef]

130. Lu, J.; Bai, X.; Zhao, Q.; Lu, B.; Fu, Y. Construction of AgI/PCN-224 Z-Scheme Heterojunction for Efficient Photocatalytic Degradation of Tetracycline Hydrochloride: Pathways, Mechanism and Theoretical Calculations. *J. Clean. Prod.* **2024**, *456*, 142364. [CrossRef]

131. Tie, W.; Bhattacharyya, S.S.; Ma, T.; Yuan, S.; Chen, M.; He, W.; Lee, S.H. Improving Photoexcited Carrier Separation through Z-Scheme W$_{18}$O$_{49}$/BiOBr Heterostructure Coupling Carbon Quantum Dots for Efficient Photoelectric Response and Tetracycline Photodegradation. *Carbon* **2024**, *231*, 119707. [CrossRef]

132. Han, M.; Wang, S.; Yu, X.; Yu, X.; Gao, H.; Zhou, X.; Li, D.; Fang, L.; Angadi V., J.; Ubaidullah, M.; et al. A Novel CuAl$_2$O$_4$/MoS$_2$/BaFe$_{12}$O$_{19}$ Magnetic Photocatalyst Simultaneously Coupling Type I and Z-Scheme Heterojunctions for the Sunlight-Driven Removal of Tetracycline Hydrochloride. *Environ. Sci. Nano* **2024**, *11*, 1948–1966. [CrossRef]

133. Zhou, T.; Dong, G.; Geng, J.; Han, K.; Xiao, C. Z-Type Composite Type II Ternary CNFeOS Heterojunction Composite Photocatalyst for Enhancing the Photocatalytic Degradation of Tetracycline. *Appl. Surf. Sci.* **2024**, *655*, 159592. [CrossRef]

134. Lu, J.; Shi, Y.; Chen, Z.; Sun, X.; Yuan, H.; Guo, F.; Shi, W. Photothermal Effect of Carbon Dots for Boosted Photothermal-Assisted Photocatalytic Water/Seawater Splitting into Hydrogen. *Chem. Eng. J.* **2023**, *453*, 139834. [CrossRef]

135. Ma, J.; Xu, L.; Yin, Z.; Li, Z.; Dong, X.; Song, Z.; Chen, D.; Hu, R.; Wang, Q.; Han, J.; et al. "One Stone Four Birds" Design Atom Co-Sharing BiOBr/Bi$_2$S$_3$ S-Scheme Heterojunction Photothermal Synergistic Enhanced Full-Spectrum Photocatalytic Activity. *Appl. Catal. B Environ.* **2024**, *344*, 123601. [CrossRef]

136. Azqandi, M.; Nateq, K.; Amarzadeh, M.; Yoosefian, M.; Yaghoot-Nezhad, A.; Ahmad, A.; Ramavandi, B.; Nasseh, N. Intensified Photo-Decontamination of Tetracycline Antibiotic by S-Scheme Spinel Manganese Ferrite-Grafted ZIF-8 Heterojunction Photocatalyst: Mechanism Conception, Degradation Pathway and DFT Studies. *J. Environ. Chem. Eng.* **2024**, *12*, 112875. [CrossRef]

137. Wang, X.; Zhang, X.; Xie, Y.; Shi, Y.; Zhao, C.; Li, G.; Zhang, Y.; Shi, H. Construction of Novel Biochar/g-C$_3$N$_4$/BiOBr Heterojunction with S-Scheme Mechanism for Efficient Photocatalytic Degradation of Tetracycline. *J. Environ. Chem. Eng.* **2024**, *12*, 113469. [CrossRef]

138. Sun, J.; Wu, H.; Fu, C.; Zhang, C.; Hu, Z.; Zhou, M. Novel Fenton-like System Based on Bifunctional MgO/g-C$_3$N$_4$ S-Scheme Heterojunction Photoanode for Efficient Tetracycline Degradation. *Appl. Catal. B Environ. Energy* **2024**, *351*, 123976. [CrossRef]

139. Alamgir; Ullah, R.; Talha, K.; Yang, H.; Mushtaq, N.; Ahmad, A.; Fan, L.; Li, L.; Zhao, G.; Wang, X.; et al. MOF-Derived In$_2$O$_3$/TiO$_2$ S-Scheme Heterojunction for Efficient Photocatalytic Degradation of Tetracycline. *J. Alloys Compd.* **2024**, *1002*, 175398. [CrossRef]

140. Chen, Z.; Ma, T.; Li, Z.; Zhu, W.; Li, L. Enhanced Photocatalytic Performance of S-Scheme CdMoO$_4$/CdO Nanosphere Photocatalyst. *J. Mater. Sci. Technol.* **2024**, *179*, 198–207. [CrossRef]

141. Beshkar, F.; Al-Nayili, A.; Amiri, O.; Salavati-Niasari, M.; Mousavi-Kamazani, M. Fabrication of S-Scheme ZnO/Zn$_3$(PO$_4$)$_2$ Heterojunction Photocatalyst toward Photodegradation of Tetracycline Antibiotic and Photocatalytic Mechanism Insight. *Int. J. Hydrog. Energy* **2022**, *47*, 928–939. [CrossRef]

142. Ding, S.; Gan, W.; Guo, J.; Chen, R.; Liu, R.; Zhao, Z.; Li, J.; Zhang, M.; Sun, Z. Construction of a SnS$_2$/TiO$_2$ S-Scheme Heterostructure Photocatalyst for Highly Efficient Photocatalytic Degradation of Tetracycline Hydrochloride. *J. Mater. Chem. C* **2024**, *12*, 7079–7094. [CrossRef]

143. Sun, L.; He, X.; Liu, B.; Zhang, S.; Xiang, Z.; Wang, X.; Wang, Y. Synergistic Adsorption-Photocatalytic Degradation of Tetracycline by S-Scheme InVO$_4$/ZnIn$_2$S$_4$ Heterojunction: Mechanism, Toxicity Assessment, and Potential Applications. *Sep. Purif. Technol.* **2025**, *353*, 128515. [CrossRef]

144. Wang, H.; Sun, S.; Ding, M.; Li, J.; Lyu, J.; Liang, S.; Cui, J. Mechanism Insight into Boosting Photocatalytic Purification of Tetracycline Hydrochloride over 2D/2D S-Scheme (BiO)$_2$CO$_3$/BiOCl Heterojunctions. *J. Environ. Chem. Eng.* **2024**, *12*, 112723. [CrossRef]

145. Huo, S.; Deng, J.; Zhao, Q.; Wang, Y.; Fu, W.; Wu, X.; Gao, M.; Xie, H. Partially Amorphization Induced S-Scheme Charge Migration in g-C$_3$N$_4$/Mn$_{1.1}$Fe$_{1.9}$O$_4$ Defective Heterojunction for Boosting Fenton-like Degradation of Tetracycline under Visible Light. *Chem. Eng. J.* **2024**, *494*, 153088. [CrossRef]

146. Liu, J.; Gong, S.; Wu, Z.; Shi, J.; Deng, H. Bi$_{3.64}$Mo$_{0.36}$O$_{6.55}$/Bi$_4$O$_5$I$_2$ S-Scheme Heterojunction Boosting Antibiotic Photodegradation: Insights from Interface to Performance. *Chem. Eng. J.* **2024**, *483*, 149156. [CrossRef]

147. Zhang, X.; Zha, X.; Luo, Y.; Liu, T.; Chen, G.; He, X. In$_2$O$_3$ Nanoparticle/Bi$_4$O$_5$Br$_2$ Nanosheet S-Scheme Heterojunctions with Interfacial Oxygen Vacancies for Photocatalytic Degradation of Tetracycline. *ACS Appl. Nano Mater.* **2023**, *6*, 11877–11887. [CrossRef]

148. Jeyaprakash, J.S.; Rajamani, M.; Bianchi, C.L.; Ashokkumar, M.; Neppolian, B. Highly Efficient Ultrasound-Driven Cu-MOF/ZnWO$_4$ Heterostructure: An Efficient Visible-Light Photocatalyst with Robust Stability for Complete Degradation of Tetracycline. *Ultrason. Sonochem.* **2023**, *100*, 106624. [CrossRef]

149. Wei, Z.; Liu, J.; Shangguan, W. A Review on Photocatalysis in Antibiotic Wastewater: Pollutant Degradation and Hydrogen Production. *Chin. J. Catal.* **2020**, *41*, 1440–1450. [CrossRef]

150. Kumar, A.; Sharma, G.; Kumari, A.; Guo, C.; Naushad, M.; Vo, D.-V.N.; Iqbal, J.; Stadler, F.J. Construction of Dual Z-Scheme g-C$_3$N$_4$/Bi$_4$Ti$_3$O$_{12}$/Bi$_4$O$_5$I$_2$ Heterojunction for Visible and Solar Powered Coupled Photocatalytic Antibiotic Degradation and Hydrogen Production: Boosting via I$^-$/I^{3-} and Bi^{3+}/Bi^{5+} Redox Mediators. *Appl. Catal. B Environ.* **2021**, *284*, 119808. [CrossRef]

151. Liu, Y.; Wang, Y.; Liu, Z.; Wang, Q. Oxidation Removal of Nitric Oxide from Flue Gas Using UV Photolysis of Aqueous Hypochlorite. *Environ. Sci. Technol.* **2017**, *51*, 11950–11959. [CrossRef]

152. Liu, Y.; Kong, J.; Yuan, J.; Zhao, W.; Zhu, X.; Sun, C.; Xie, J. Enhanced Photocatalytic Activity over Flower-like Sphere Ag/Ag$_2$CO$_3$/BiVO$_4$ Plasmonic Heterojunction Photocatalyst for Tetracycline Degradation. *Chem. Eng. J.* **2018**, *331*, 242–254. [CrossRef]

153. Ding, Y.; Ye, Y.; Wang, C.; Pei, L.; Mao, Q.; Liu, M.; Zheng, R.; Bokhari, A.; Han, N.; Zhong, J. "Light Battery" Role of Long Afterglow Phosphor for Round-the-Clock Environmental Photocatalysis. *J. Clean. Prod.* **2024**, *450*, 142041. [CrossRef]

154. Wei, Y.; Liu, Y.-B.; Liu, C.; Li, X.; Zhao, G.-H.; Liu, R.-H.; Wang, H.-Y.; Jiang, Y.-Y.; Zhang, Y.-L.; Gao, Y.-H.; et al. Construction of Oxygen-Doped g-C$_3$N$_4$/BiOCl (S-Scheme) Heterojunction: Efficient Degradation of Tetracycline in Wastewater. *J. Environ. Chem. Eng.* **2024**, *12*, 113354. [CrossRef]

155. Xu, Z.; Jin, X.; Zhong, J.; Li, M.; Zhang, S. In-Situ Fabrication of BiOCl/OVs–BiPO$_4$ Heterojunctions with Enhanced Photocatalytic Destruction Performance. *Rare Metals* **2024**, 1–16. [CrossRef]

156. Wang, A.; Liang, H.; Chen, F.; Tian, X.; Jing, S.; Tsiakaras, P. Preparation and Characterization of Novel NiIn$_2$S$_4$/UiO-66 Photocatalysts for the Efficient Degradation of Antibiotics in Water. *Chemosphere* **2022**, *307*, 135699. [CrossRef]

157. Yang, R.; Fan, Y.; Zhang, Y.; Mei, L.; Zhu, R.; Qin, J.; Hu, J.; Chen, Z.; Ng, Y.; Voiry, D.; et al. 2D Transition Metal Dichalcogenides for Photocatalysis. *Angew. Chem. Int. Ed.* **2023**, *62*, e202218016. [CrossRef]

158. Zhao, H.; Li, G.; Tian, F.; Jia, Q.; Liu, Y.; Chen, R. G-C3N4 Surface-Decorated Bi$_2$O$_2$CO$_3$ for Improved Photocatalytic Performance: Theoretical Calculation and Photodegradation of Antibiotics in Actual Water Matrix. *Chem. Eng. J.* **2019**, *366*, 468–479. [CrossRef]

159. Zhou, Y.; Jiang, D.; Wang, Z.; Yi, L.; Sun, J.; Liu, D.; Yu, X.; Chen, Y. Bandgap Engineering of Carbon Nitride by Formic Acid Assisted Thermal Treatment for Photocatalytic Degradation of Tetracycline Hydrochloride. *Chem. Eng. J.* **2024**, *485*, 149830. [CrossRef]

160. Hu, X.; Zhang, Z.; Lu, P.; Zhou, Y.; Zhou, Y.; Bai, Y.; Yao, J. Cyano-Deficient g-C$_3$N$_4$ for Round-the-Clock Photocatalytic Degradation of Tetracycline: Mechanism and Application Prospect Evaluation. *Water Res.* **2024**, *260*, 121936. [CrossRef]

161. Fu, X.; Kong, Y.; Wang, M.; Cai, T.; Zeng, Q. MXene Derived Ti$_3$C$_2$/TiO$_2$/Ag Persistent Photocatalyst with Enhanced Electron Storage Capacity for Round-the-Clock Degradation of Organic Pollutant. *J. Colloid Interf. Sci.* **2024**, *656*, 233–240. [CrossRef]

162. Shi, J.; Xu, Y.; Chen, Y.; Jiang, W.; Liu, B.; Pei, W.; Liu, C.; Zhou, T.; Che, G. In-Site Growing Honeycombed Integrated S-Doped-g-C$_3$N$_4$-NiCo$_2$O$_4$ PMS Activator for Round-the-Clock Ultra-Efficient Degradation of Multiple Pollutants. *Sep. Purif. Technol.* **2025**, *354*, 129492. [CrossRef]

163. Wu, C.; Lv, K.; Li, X.; Li, Q. Dual Cocatalysts for Photocatalytic Hydrogen Evolution: Categories, Synthesis, and Design Considerations. *Chin. J. Catal.* **2023**, *54*, 137–160. [CrossRef]

164. Ma, L.; Lu, M.; Li, K.; Zhang, S.; Liu, H.; Huang, Y.; Xing, Z.; Wu, Z.; Ye, X. Photocatalytic Degradation of Octadecylamine and 4-Dodecylmorpholine over Titanium Based Photocatalyst: Activity and Mechanism Insights. *Chem. Eng. J.* **2023**, *472*, 144782. [CrossRef]

165. Chen, R.; Ni, C.; Zhu, J.; Fan, F.; Li, C. Surface Photovoltage Microscopy for Mapping Charge Separation on Photocatalyst Particles. *Nat. Protoc.* **2024**, *19*, 2250–2282. [CrossRef]

166. Wang, Z.; Cheng, Q.; Wang, X.; Li, J.; Li, W.; Li, Y.; Zhang, G. Carbon Dots Modified Bismuth Antimonate for Broad Spectrum Photocatalytic Degradation of Organic Pollutants: Boosted Charge Separation, DFT Calculations and Mechanism Unveiling. *Chem. Eng. J.* **2021**, *418*, 129460. [CrossRef]

167. Fang, Y.; Liu, Y.; Huang, H.; Sun, J.; Hong, J.; Zhang, F.; Wei, X.; Gao, W.; Shao, M.; Guo, Y.; et al. Design and Synthesis of Broadband Absorption Covalent Organic Framework for Efficient Artificial Photocatalytic Amine Coupling. *Nat. Commun.* **2024**, *15*, 4856. [CrossRef]

168. Tao, X.; Zhou, H.; Zhang, C.; Ta, N.; Li, R.; Li, C. Triclinic-Phase Bismuth Chromate: A Promising Candidate for Photocatalytic Water Splitting with Broad Spectrum Ranges. *Adv. Mater.* **2023**, *35*, 2211182. [CrossRef]

169. Zhou, P.; Navid, I.A.; Ma, Y.; Xiao, Y.; Wang, P.; Ye, Z.; Zhou, B.; Sun, K.; Mi, Z. Solar-to-Hydrogen Efficiency of More than 9% in Photocatalytic Water Splitting. *Nature* **2023**, *613*, 66–70. [CrossRef]

170. Sathish, T.; Saravanan, R.; Kumar, A.; Prakash, C.; Shahazad, M.; Gupta, M.; Senthilkumar, N.; Pandit, B.; Ubaidullah, M.; Smirnov, V.A. Influence of Synthesizing Parameters on Surface Qualities of Aluminium Alloy AA5083/CNT/MoS$_2$ Nanocomposite in Powder Metallurgy Technique. *J. Mater. Res. Technol.* **2023**, *27*, 1611–1629. [CrossRef]

171. Suganya, B.; Maruthamuthu, S.; Chandrasekaran, J.; Saravanakumar, B.; Vijayakumar, E.; Marnadu, R.; Al-Enizi, A.M.; Ubaidullah, M. Design of Zinc Vanadate (Zn$_3$V$_2$O$_8$)/Nitrogen Doped Multiwall Carbon Nanotubes (N-MWCNT) towards Supercapacitor Electrode Applications. *J. Electroanal. Chem.* **2021**, *881*, 114936. [CrossRef]

172. Ubaidullah, M.; Ahmed, J.; Ahamad, T.; Shaikh, S.F.; Alshehri, S.M.; Al-Enizi, A.M. Hydrothermal Synthesis of Novel Nickel Oxide@nitrogenous Mesoporous Carbon Nanocomposite Using Costless Smoked Cigarette Filter for High Performance Supercapacitor. *ACS Mater. Lett.* **2020**, *266*, 127492. [CrossRef]

173. Zhao, Y.; Qiao, L.; Zhang, M.; Xiao, Y.; Tao, Y.; Yang, F.; Lin, Q.; Zhang, Y. Roles of BOCu Sites and Graphite Nitrogen on Persulfate Non-Radical Activation for Tetracycline Degradation. *J. Colloid Interface Sci.* **2024**, *673*, 178–189. [CrossRef]

174. Chen, P.; Cheng, Z.; Zhang, X.; Yan, C.; Wei, J.; Qiu, F.; Liu, Y. Fe–Mn Bimetallic Catalyst to Activate Peroxymonosulfate (PMS) for Efficient Degradation of Tetracycline: Mechanism Insights and Application for Pharmaceutical Wastewater. *J. Clean. Prod.* **2024**, *445*, 141365. [CrossRef]

175. Tan, J.; Li, Z.; Li, J.; Meng, Y.; Yao, X.; Wang, Y.; Lu, Y.; Zhang, T. Visible-Light-Assisted Peroxymonosulfate Activation by Metal-Free Bifunctional Oxygen-Doped Graphitic Carbon Nitride for Enhanced Degradation of Imidacloprid: Role of Non-Photochemical and Photocatalytic Activation Pathway. *J. Hazard. Mater.* **2022**, *423*, 127048. [CrossRef] [PubMed]

176. Yuan, M.; Zhu, Y.; Fu, J.; Xu, S.; Wu, X.; Wang, Z.; Yuan, M.; Song, Z.; Cui, S. Facile Synthesis of a Novel Zn$_2$Ti$_3$O$_8$ Aerogel with Porous Structure for High-Efficient Degradation of Antibiotics under Simulated Sunlight. *Ceram. Int.* **2023**, *49*, 23264–23275. [CrossRef]

177. Qiu, J.; Peng, C.; Wang, R.; Yao, C.; Liu, X.; Wang, Q.; Wang, W. One-Step in-Situ Preparation of C/TiO$_2$@rGO Aerogel Derived from Ti$_3$C$_2$T$_x$ MXene for Integrating Microwave Absorption, Electromagnetic Interference Shielding and Catalytic Degradation of Antibiotics. *Carbon* **2024**, *217*, 118610. [CrossRef]

178. Zhang, W.; Liu, H.; Chen, Z.; Yang, Z.; Zhang, X.; Wang, X. In Situ Construction of CdS/g-C$_3$N$_4$ Heterojunctions in Spent Thiolation@Wood-Aerogel for Efficient Excitation Peroxymonosulfate to Degradation Tetracycline. *ACS Appl. Mater. Interfaces* **2024**, *16*, 28353–28366. [CrossRef]

179. Xiao, M.; Wang, Z.; Lyu, M.; Luo, B.; Wang, S.; Liu, G.; Cheng, H.-M.; Wang, L. Hollow Nanostructures for Photocatalysis: Advantages and Challenges. *Adv. Mater.* **2019**, *31*, 1801369. [CrossRef]

180. Liu, J.; Dong, Y.; Zhang, Y.; Liu, W.; Xu, J.; Lin, H. Enhanced Synergistic Performance of G-C$_3$N$_4$/MoS$_2$ with Hollow Structure for Tetracycline Photocatalytic Degradation in Complex Environments: Performance and Mechanism. *J. Clean. Prod.* **2024**, *451*, 141983. [CrossRef]

181. Luo, T.; Bao, Y. Stable Fabrication of S-Step Photocatalyst Assembled from Cu-Doped SnO$_2$ Yolk-Shell Hollow Spheres Capsulated by MnCo$_2$O$_4$ Nanoparticles for Enhancing Antibiotic Photodegradation. *Sep. Purif. Technol.* **2024**, *347*, 127503. [CrossRef]

182. Wu, X.; Zhang, C.; Nie, Z.; Zhang, Y.; Bai, Q.; Yin, Z.; Zhang, S.; Qu, X.; Du, F.; Shi, L. Cookies-like Ag$_2$S/Bi$_4$NbO$_8$Cl Heterostructures for High Efficient and Stable Photocatalytic Degradation of Refractory Antibiotics Utilizing Full-Spectrum Solar Energy. *Sep. Purif. Technol.* **2022**, *292*, 120969. [CrossRef]

183. Sun, H.; Wang, C.; Shao, Y.; Zhang, Y.; Chen, C.; Liu, H.; Dou, S.; Xu, J.; Zhang, Y.; Lou, Y.; et al. Balanced Generation of Holes and Superoxide Radicals on $Bi_{25}CoO_{40}$ Sillenite Photocatalysts for Rapid Synergetic Degradation of Quinolone Antibiotics. *Environ. Sci. Nano* **2024**, *11*, 3178–3191. [CrossRef]

184. Li, L.; Xu, M.; Deng, Y.; Zheng, J.; He, C.; Tremblay, P.L.; Zhang, T. Photocatalytic degradation of persistent antibiotic pollutants by MOF-derived bird-nest ferric molybdate. *J. Water Process Eng.* **2024**, *60*, 105166. [CrossRef]

185. Song, R.; Chi, H.; Ma, Q.; Li, D.; Wang, X.; Gao, W.; Wang, H.; Wang, X.; Li, Z.; Li, C. Highly Efficient Degradation of Persistent Pollutants with 3D Nanocone TiO_2-Based Photoelectrocatalysis. *J. Am. Chem. Soc.* **2021**, *143*, 13664–13674. [CrossRef] [PubMed]

186. He, P.; Zhu, H.; Ma, Y.; Liu, N.; Niu, X.; Wei, M.; Pan, J. Rational Design and Fabrication of Surface Molecularly Imprinted Polymers Based on Multi-Boronic Acid Sites for Selective Capture Glycoproteins. *Chem. Eng. J.* **2019**, *367*, 55–63. [CrossRef]

187. Lu, Z.; Ren, Y.; Wang, P.; Xu, Y.; Zhang, J.; Wei, B.; Zhou, G.; Liu, X.; Huang, Y.; Wu, C. High-Throughput Imprinted Non-Metal S-Scheme Heterojunction Self-Cleaning Membrane with Tight Adhesion via Dopamine for Selective Photodegradation of TC. *J. Environ. Chem. Eng.* **2023**, *11*, 109745. [CrossRef]

188. Fu, J.; Li, S.; Li, Q.; Bell, E.; Yang, D.; Li, T.; Li, Y.; He, J.; Zhou, L.; Zhang, Q.; et al. Preparation of Surface Molecular-Imprinted MOFs for Selective Degradation of Tetracycline Antibiotics in Wastewater. *Colloids Surf. Physicochem. Eng. Asp.* **2024**, *687*, 133575. [CrossRef]

189. Li, J.; Li, Z.; Song, Y.; Zhang, X.; Xie, H.; Sheng, S.; Zou, H. 3D/1D $Fe_3O_4@TiO_2/TC$-TiO_2/SiO_2 Magnetic Inorganic-Framework Molecularly Imprinted Fibers for Targeted Photodegradation. *Inorg. Chem.* **2024**, *63*, 10568–10584. [CrossRef] [PubMed]

190. Yuan, Y.; Zhu, X.; Liu, Y.; An, Z.; Jia, H.; Wang, J. Design of Membrane-Based Microfluidic Chip Device Based on Bionic Leaf and Adsorption Detection of Tetracycline Antibiotics by Specific Gel Membrane. *Chem. Eng. J.* **2024**, *495*, 153394. [CrossRef]

191. Liu, X.; Wang, Y.; Wang, Q.; Yang, W. Chloroplast Inspired Z-Scheme Photocatalyst for Efficient Degradation of Antibiotics: Synergistic Effect of Full-Visible Light Response, Multi-Channel Electron Transport and Enhanced Molecular Oxygen Activation. *Sep. Purif. Technol.* **2023**, *315*, 123721. [CrossRef]

192. Ortiz, M.; Gomez, E.; Serra, A. Recyclable Biomimetic Sunflower Pollen-Based Photocatalyst for Enhanced Degradation of Pharmaceuticals. *Small* **2024**, 2405204. [CrossRef]

193. Xia, C.; Ou, X.; Chen, P.; Zhang, F.; Wei, M.; Wang, Y.; Zhang, M. Sunlight Degradation of Tetracycline by Z-Type $BiOI/g$-C_3N_4 Photocatalyst Synthesized via a Simple Two-Step Process: Response Surface Methods, Degradation Pathways, Toxicity Evaluation. *J. Water Process Eng.* **2024**, *64*, 105617. [CrossRef]

194. Liu, X.; Wang, H.; Wang, C.; Zhao, L.; Pan, H.; Liu, Y.; Liang, L.; Zhao, C.; Huang, S. Self-Endowed Magnetic Photocatalysts Derived from Iron-Rich Sludge and Its Recycling in Photocatalytic Process for Tetracycline Degradation. *Bioresour. Technol.* **2024**, *395*, 130357. [CrossRef] [PubMed]

195. Pajouhan, Y.; Sabbaghi, S.; Rasouli, K.; Rasouli, J.; Dastyar, W.; Andiroglu, E. Enhanced Photocatalytic Degradation of Tetracycline Using α-$Fe_2O_3@TiO_2$- Impregnated Mxene Photocatalyst: Mechanism and Optimization of Process via RSM and ANN. *Process Saf. Environ.* **2024**, *190*, 1149–1163. [CrossRef]

196. Xue, B.; Yang, C.; Chang, M.; Liu, D. Structural Design of Core-Shell ZIF-8@NH_2-MIL-125 Photocatalyst for Synergistic Adsorption-Photocatalytic Degradation of Tetracycline Hydrochloride. *J. Alloys Compd.* **2024**, *973*, 172850. [CrossRef]

197. Luo, X.; Zhu, P.; Xie, T.; Liang, T.; Qiu, Q. Oxygen Vacancy and Ce Ion Co-Synergize to Enhance the Photocatalytic Degradation Performance of $FeTiO_3$: An Experimental and DFT Study. *Appl. Surf. Sci.* **2024**, *669*, 160415. [CrossRef]